POLITECNICO DI TORINO

Master's degree course in
Communications and Computer Networks Engineering

Master's degree Thesis

RF Multipath Estimation in GPS Signals using Dual Polarised Antenna (DPA)

Supervisor:
Prof. Ladislau Matekovits

Candidate:
Ajita Khanal

Co-Supervisors:
Dr. Livio Marradi
Ph.D. Andrea Emmanuele
Dr. Marco Puccitelli

A.A. 2018/2019

Abstract

The GPS signals travelling through space come across various phenomena before reaching the receiver. Multipath, one of these effects, indicate the situation when the GPS signals propagating towards the receiver undergo reflection on the ground or surrounding objects and reach the receiver not only through one path but also these secondary components. This causes the receiver to collect the Line of Sight (LoS) signal along with the reflected version of the signal which arrives with a certain amount of delay, modified also in amplitude and phase based on reflecting surface.

This results in error in the so called “pseudo-range” estimation, i.e. the distance between satellite transmitting the signal and the receiver. The composite signal received due to the multipath contributions has various characteristics in terms of amplitude, polarisation, phase and delay. These characteristics mainly depend on the kind of the reflecting material that the signal comes across.

This thesis focuses on the study of the GNSS signals, in particular GPS L1CA is considered here as case of study, received using a dedicated platform consisting of a Dual Polarised Antenna (DPA) and a High Sensitive Receiver (HS RX). The DPA is in charge to provide received GNSS signals in both the Right Hand Circular Polarisation (RHCP), i.e. the polarisation which is currently used for GNSS signals transmitted at satellite level, and Left Hand Circular Polarisation (LHCP) components. The HS receiver has the capability to be fed and to process up to two RF inputs, which have been used to process the two DPA outputs, i.e. RHCP and LHCP signals. For this purpose, the receiver has been configured in a “sensitivity mode” to acquire and track the LHCP signals, assumed to carry lower power than typical RHCP GNSS signals.

Another main feature of the receiver adopted for the study has been the capability to generate a multiple number of correlators, for each of the used branches (one for RHCP and the other for LHCP signals) instead of the conventional Early - Late and Prompt correlators.

In this thesis an innovative technique for multipath parameter estimation has been designed and configured, working at post-correlation level, taking benefit of the available multiple correlation values coming from both RHCP and LHCP polarisations.

The In phase and Quadrature-phase components (I/Q) of all the eleven multicorrelators received from both the RHCP and LHCP chains are analysed and processed to see the characteristics of the signal received and tracked. The signals at post-correlation level have been modelled accounting for the specific receiver architecture, in particular, considering that LHCP tracking was independent of the RHCP one. Furthermore, a tracking error was considered between the two branches.

After a preliminary analysis about the characteristics of the multicorrelator observables available (e.g. noise variance estimation), and a review of the state-of-the art algorithms available in literature, an Extended Kalman Filter (EKF) scheme has been chosen matching the target of estimating multipath parameters in a GNSS environment.

The performance of the EKF in parameters estimation depends on the correctness of the model developed to represent the signals and states to be estimated. Hence, one of the main focuses of this work has been to model and characterise the multipath signal by taking the advantage of both RHCP and LHCP sensed polarisations.

Along with the conventional EKF, a constrained version of the EKF has been analysed, using the two RHCP and LHCP Delay Lock Loop (DLL) discriminator properties, i.e. lock points where difference between Early and Late correlators is zero on average. A DLL is a particular scheme in the receiver, in charge of estimating the delay parameter in a closed loop architecture. Similar scheme is defined for a Phase Lock Loop (PLL) and a Frequency Lock Loop (FLL), for phase and frequency parameter estimation, respectively.

Finally, results are reported in the work depicting the EKF estimates as the amplitude, delay and phase for LoS and the multipath component for both the RHCP and LHCP branches for each GPS signal received. Various Figures of Merit (FoM) have been considered as combination of the EKF estimates. The statistics and time evolutions have been used in order to characterize the FoM, like the D/U ratio (i.e. ratio between desired and undesired signals) between estimated received RHCP and LHCP multipath components with respect to the estimated received RHCP and LHCP LoS signal components. Taking advantage of these figures of merit and statistics output of the EKF scheme here analysed, the presence of multipath has been detected and its parameters characterized in a set of live environments.

In the frame of this work, live databases with real signals have been acquired and stored with DPA antenna and HS Receiver, in order to verify the algorithm performance in presence of real multipath environment.

In particular, the data to be processed in the thesis work have been acquired in the premises of European Space Agency (ESA/ESTEC) in Noordwjik, the Netherlands, on top of a roof in presence of several reflectors. The entire work of the thesis has been performed in Thales Alenia Space Italia (TASI), Gorgonzola (Milan) and results have been already published in [1].

Finally, the work has been carried out in TASI in the frame of the ESA contract n. 4000122396/17/NL/CRS/hh, “Toolbox for Multipath Survey based on GNSS Dual Polarized Antenna”. The content of the thesis reflects solely the authors’ view and by no means represents the official TAS-I view, ESA view or the one from ESA Galileo and EGNOS Project Offices.

Acknowledgements

I would like to begin by thanking my supervisor, Mr. Andrea Emmanuele, for his guidance and continuous support during my internship at Thales Alenia Space Italia, without whom the thesis would not have been possible. I am very grateful to Mr. Livio Marradi for providing me with this opportunity to be a part of such an interesting project in which I had the chance to learn so much. My sincere thanks goes to Mr. Marco Puccitelli for his valuable help throughout the project. I feel very gratified towards my professor at Politecnico di Torino, Mr Ladislau Matekovits, for his constant support and availability at any time.

I am indebted towards my parents for everything that they have done for me and for always believing in me. I would like to thank my sister who I have always admired for teaching me patience and the importance of hard work. A special thanks to my brother for being so funny and cheering me up in the times of stress. I am sincerely very thankful towards Mariella, Ettore and Roberto at Thales Alenia Space for their endless moral support and for being my family away from home. I am immensely grateful to my friends Astha, Birat, Prakash, Davide, Giulio, Andrea and Cristina for encouraging and upholding me throughout this journey.

Table of Contents

List of Figures

List of Abbreviations

BOC	Binary Offset carrier
BPSK	Binary Phase Shift Keying
CBOC	Composite binary offset carrier
CDMA	Code Division Multiple Access
C-EKF	Constrained Extended Kalman Filter
DLL	Delay Locked Loop
DoD	Department Of Defence
DPA	Dual Polarised Antenna
E	Early
EM	Electro Magnetic
EKF	Extended Kalman Filter
GNSS	Global Navigation Satellite Systems
GPS	Global Positioning Systems
HS	High Sensitivity
L	Late
LHCP	Left Hand Circular Polarisation
LoS	Line of Sight
MBOC	Modernized Binary Offset Carrier
MET	Multipath Elimination Technology
NC	Narrow Correlators
NLoS	Non Line of Sight
PICC	Parallel Iterative Cross Cancellation

PPP	Precise Point Positioning
PLL	Phase Locked Loop
PRN	Pseudo Random Noise
RF	Radio Frequency
RHCP	Right Hand Circular Polarisation
RTK	Real Time Kinematic
SBAS	Space Based Augmentation Systems
TMBOC	Time Multiplexed Binary Offset Carrier

List of symbols

E	Electric Field Vector
E_h	Horizontal component of Electric Field Vector
E_v	Horizontal component of Electric Field Vector
θ_g	Grazing angle
Ψ_B	Brewster Angle
δ	Relative Delay
$s(t)$	Received composite signal
$a_i(t)$	amplitude of the i^{th} component
$p(t)$	GNSS signal modulation
$\tau_i(t)$	relative delay of the i^{th} component
ω_0	Nominal frequency of the LoS signal
$\theta_i(t)$	relative phase of the i^{th} component
$\epsilon(t)$	Noise
$s_{LoS}(t)$	LoS signal component
$s_{MP}(t)$	Multipath signal component
α	ratio between multipath and direct signal amplitude
LOS_1	Line of sight component in RHCP chain
MP_R	RHCP multipath component
MP_L	LHCP multipath component
G_R	Co-polar gain
G_{XR}	Cross polar gain
Γ	reflection coefficient
P	signal power

d	navigation bit
f	GPS signal carrier frequency
c	C/A code sequence
τ_0	Code delay for the LOS signal
τ_{MP}	Code delay for the Multipath signal
α_{LOS}^{RR}	LOS signal amplitude at RHCP
ϕ_{LOS}^{RR}	Average phase error for the LOS signal
α_{MP}^{R}	RHCP multipath amplitude
$\delta\phi_{\mathrm{MP}}^{R}$	Average phase error for the RHCP Multipath signal
$\delta\tau_{LOS}^{R}$	error in LoS delay estimation
$\tau_{LOS}^{'}$	The measured LoS delay at RHCP chain
τ_{LOS}^{R}	The actual LoS delay .
$\delta\tau_{MP}^{R}$	The relative multipath tracking error at RHCP
α_{LOS}^{LR}	RHCP LoS signal amplitude at LHCP
$\delta\phi_{\mathrm{LOS}}^{LR}$	Average phase error for the LOS signal
α_{MP}^{L}	LHCP multipath amplitude
$\delta\phi_{\mathrm{MP}}^{L}$	Average phase error for the LHCP Multipath signal
$\tau_{LOS}^{''}$	Measured LoS delay at LHCP chain
x_k	vector of states
z_k	measurement vector
z_k	measurement noise
w_k	process noise
v_k	measurement noise
F	state transition matrix
Q	Process noise covariance matrix

H	observation matrix
R	measurement noise covariance matrix
P_k	posteriori covariance matrix
K_k	Kalman gain
C/No	Carrier to noise ratio

1 INTRODUCTION AND OVERVIEW

1.1 INTRODUCTION TO GNSS

Satellite navigation system refers to the system that makes the use of the signals transmitted by the satellites in order to provide the position of an object. In the early age, navigators depended on celestial observations to determine time and position of the objects on the Earth. However, in the modern systems positions are ascertained through the receivers that collect the signals from the satellites. The position is determined by the means of the propagation time of the signals, phase and the received signal strength.

The very first modern satellite navigation system designed was the NAVSTAR Global Positioning System (GPS) managed by the Department of Defence (DoD) of the United States of America. Today there are other navigation systems among which Global Navigation Satellite System (GLONASS) owned by the Russian Federation is fully operational. Europe has its own navigation system, Galileo, managed by the European Union, which is still under development. Today without the existence of the navigation systems the vehicles commuting on the road, ships, aircrafts, and many people around the world would be lost. Apart from this various safety, security and emergency operations would be absolutely paralyzed [2].

These systems that we have become fully dependent on relies on the signals transmitted by the GNSS satellites. These signals are a combination of carrier, ranging code called as Pseudo-Random Noise (PRN) sequence and navigation data. The information carried by these signals are used to compute the position of the receiver. A more detailed description of the GNSS signals, in particular, GPS signals and their characteristics is presented in chapter two.

The navigation systems encounter various error sources during propagation and even in the satellites during generation and at the receiver during the reception. The inaccuracy of satellite clocks even by the slightest causes a significant error in position calculation. The satellites travel in their known fixed orbits which are nearly precise but there are some variations that cause orbital errors. The clock errors and orbital errors can be compensated with the help of corrections from Precise Point Positioning (PPP) service or the Space Based Augmentation System (SBAS). Other ways by which these errors can be compensated are Differential GNSS or Real Time Kinematic (RTK) receiver configuration [3].

The GNSS signals also experience errors due to ionospheric delay when they come across the layer of ionosphere while travelling from the space towards the earth's surface. This delay varies on the time of the day, year and the level of ionospheric activity. These errors can be easily compensated in dual frequency receivers, while for signal frequency receivers, ionospheric models can be implemented for estimation and compensation of the delay. After ionosphere the signals encounter the layer of troposphere where they undergo further delay because of the pressure, temperature and humidity in the atmosphere. These errors too can be compensated with the help of differential GNSS and RTK systems.

The error sources that we discussed so far can be compensated in some way or the other. However, the class of error source caused by the multipath phenomena, which is the focus of the thesis, is the most difficult one to mitigate. Multipath is a phenomenon in which the transmitted signal reaches the receiving antenna not only through the Line of Sight (LoS) but also by the means of indirect paths. These unwanted signals that arrive in the receiver with a certain delay, phase and amplitude relative to the LoS signals gets combined with the LoS signal causing them to be distorted. This causes severe tracking errors resulting in the degradation of positioning accuracy.

The severity of multipath effect depends on the kind of application we are talking about. It could be unacceptable for the applications with precise positioning requirements like autonomous driving and defence whereas an airplane using GNSS for en voyage navigation can deal with several 100 metres of positioning error [4]. This error source is very difficult to mitigate as it is very different for even receivers with small physical separation. Moreover, even the differential corrections cannot remove the multipath errors in receiver that are close to each other because of their area-dependent features. Various multipath mitigation techniques at antenna level, post correlation level and measurement post processing levels have been introduced in the literature. A detailed description of these techniques is presented in chapter 3. Considering the necessity of characterisation of multipath, a technique for estimating multipath parameters has been implemented and analysed in this thesis.

1.2 OBJECTIVE OF THE THESIS

The main purpose of this thesis work has been to develop an algorithm able to characterize multipath by estimating its main parameters, basing on the outputs of multi-correlator technology of a High Sensitivity (HS) receiver connected to a Dual Polarized Antenna (DPA) to produce RHCP and LHCP observables. The work developed in the thesis is a part of a much larger toolbox which works in post processing mode with variety of functionalities. The toolbox works in the open loop mode and hence no feedbacks are provided to the runtime receiver processing chain. The toolbox is designed to be used to survey potential sites for GNSS ground reference stations, monitoring for the presence of multipath and Radio Frequency (RF) interferences.

One task of the thesis has been to provide a detailed theoretical background on the multipath and its effects on the GPS signal processing performance at receiver side. It also discusses about the existing methodologies that have been implemented for characterisation, mitigation and estimation

of multipath. The signals analysed for multipath estimation have been legacy GPS L1CA ones, received and processed in order to obtain multicorrelators at receiver side, fed by Dual Polarised antenna (DPA). A scenario of a single multipath reflection is considered and modelled. It focuses on the multipath characterisation and parameters estimation by feeding In-phase (I) and Quadrature-phase (Q) multicorrelators samples to an Extended Kalman Filter (EKF) by taking an advantage of RHCP-LHCP polarisation diversity offered by the DPA.

The modelling of the composite GPS signal received and the multipath parameters to be estimated by the EKF is a fundamental part of the thesis. The work provides a detailed description on the EKF operations and an idea of design of the *noise matrices* and the *transition ones*, that are required to be fed to the Kalman filter throughout its three basic steps of prediction, correction and update. Apart from the conventional EKF a constrained version is further introduced in the thesis, by embedding a constraint on both the RHCP and LHCP receiver chains. The results generated for both the cases are then analysed, discussed and compared.

The core part of the project begins with the analysis and processing of the received data which are then fed to the EKF algorithm for estimation. The purpose of the thesis has been so to generate a series of charts depicting the evolution of the states along time and the histograms to also provide for statistical analysis of the estimates. The figures include the representation of the estimated LoS and multipath signal amplitudes , LoS and multipath delay and phases for both the RHCP and LHCP chains. In addition to this, other figures of merit like D/U ratios (ratio between the desired and undesired signals) along with the histograms for both the chains are reported and discussed. A statistical characterisation of all the ratios between the multipath amplitudes estimated at the RHCP and LHCP reception chains w.r.t. the LoS amplitude (at the RHCP and LHCP chains) are presented and discussed.

1.3 OUTLINE OF THE THESIS

This chapter provided a basic description of the Navigation systems, GNSS signals and the errors that the signals goes through at different levels. This chapter also gives a brief overview of the work performed in the thesis.

Chapter two provides a detailed description of the GPS signals, in particular the GPS L1CA signals as all the analysis done in the thesis is based on this one. Along with this, it also provides a discussion on the polarisation of the GPS signals and the change in polarisation that could incur on the signal after multipath. It also discusses the influence of the reflecting material on the change in original polarisation of the signal.

Chapter three discusses the necessity of the multipath characterisation and mitigation. It provides a brief information on the existing methodologies that have been implemented in order to characterise, mitigate and estimate the multipath environment and its parameters.

Chapter four deals with the illustration and analysis of the real data received from the receiver. After this, the RHCP and LHCP signals model are defined and reported. In particular, signal composition is defined as the LoS signal and a single echo. All the steps considered in the modelling of the signals at both RHCP and LHCP are described step by step in detail and the definition of the parameters to be estimated is provided. Finally, a relationship between the RHCP and LHCP model is illustrated with the help of a self- explanatory figure.

Chapter five provides a review of the techniques used in the thesis. It provides a detailed description of the EKF steps and a constrained version of the EKF and the motivation that led to the use of EKF scheme. In this chapter the modelling of the parameters defined in chapter four is performed. In this chapter the parameters to be estimated are modelled, the considerations taken into designing the process noise covariance matrix (Q), the measurement noise matrix (R) , the

initial state vector, the estimation covariance matrix (P) are described. Along with their design it also describes the importance of their proper design in the convergence of the EKF.

Chapter six provides a detailed set up description which includes the description of the antenna, the receiver and its processing, in order to acquire/track the signals analysed in the thesis. It also provides a basic flow of the toolbox with the help of some dialog boxes that the user has to make choices from in order to perform the analysis. As it was said that the work done in the thesis is a part of a more diverse toolbox, only the EKF estimation algorithm is considered here in its flow description.

Chapter seven deals with the analysis of the techniques reviewed in chapter five. The results are reported, and an analysis and discussion of them is performed. All the charts and figures of merits that have been named in the *§1.2* are illustrated and discussed. It also includes a statistical analysis of some figures of merits. At first the results obtained by subjecting the I/Q multicorrelators observables to the EKF are presented and analysed. After this the same is done for the constrained version of the EKF. A comparison of the results obtained from these two processes for the same PRN is done.

Finally, chapter eight provides the conclusions of the thesis work. In this chapter a short summary of the thesis has been presented, including possible future works that can be done on the algorithm currently developed.

2 GPS SIGNALS AND SIGNAL POLARISATION

2.1 GPS SIGNALS

GPS signals are RF electromagnetic (EM) waves broadcasted by the navigation satellites. These signals allow the user to estimate the pseudo range between the user and the satellite identified by it. These signals along with the ranging information also carries the navigation data. These signals can identify the satellite broadcasting them in a unique way by using Code Division Multiple Access (CDMA) technique. Each GPS satellite transmits a different ranging code using the same carrier frequencies. The codes that they transmit are mutually orthogonal to each other so that the GPS receivers can distinguish the signal of interest from others.

Each signal consists of 3 components:

1. **Carrier** : It is the RF sinusoidal signal with frequency f_{L1} (L1 = 1575.42 MHz)and f_{L2}(L2 = 1227.60 MHz) in the L band. The frequencies are derived from the value 10.23 MHz. In GPS all the signals and codes are driven by a unique clock of 10.23 MHz in order to guarantee synchronisation. There are also other classified signals transmitted at L3 and L4.
2. **Ranging code** : Each satellite transmits 2 codes
    - **Coarse/Acquisition code (C/A)** : The C/A codes are gold codes of 1 milli seconds (ms) that allows the fast but not precise acquisition of the signal. The length of the code is 1023 chips with the chip duration of 1μs.
    - **Precision [encrypted] code (P)[(Y)]** : The P codes have a greater precision because they have a shorter chip time compared to the C/A codes. The code length is extremely long. The duration of the code is 1 week, and the chip rate is 10.23 Mega

chips per second (Mchips/s). The P code can also be replaced with a secure Y-code which provides an additional anti spoof mode for authorized U.S. Government users.

3. **Navigation data**: The C/A code and P code are combined with a binary navigation data. The navigation data is a binary coded message carrying information on the health status of the satellites, the ephemeris parameters, the SV clock bias parameters, relativistic corrections, ionospheric model parameters and almanac data. The navigation data has a bit rate of 50 bits per second (bits/s) and a bit duration of 20 ms.

The combination of the 3 signals can be shown by the figure below

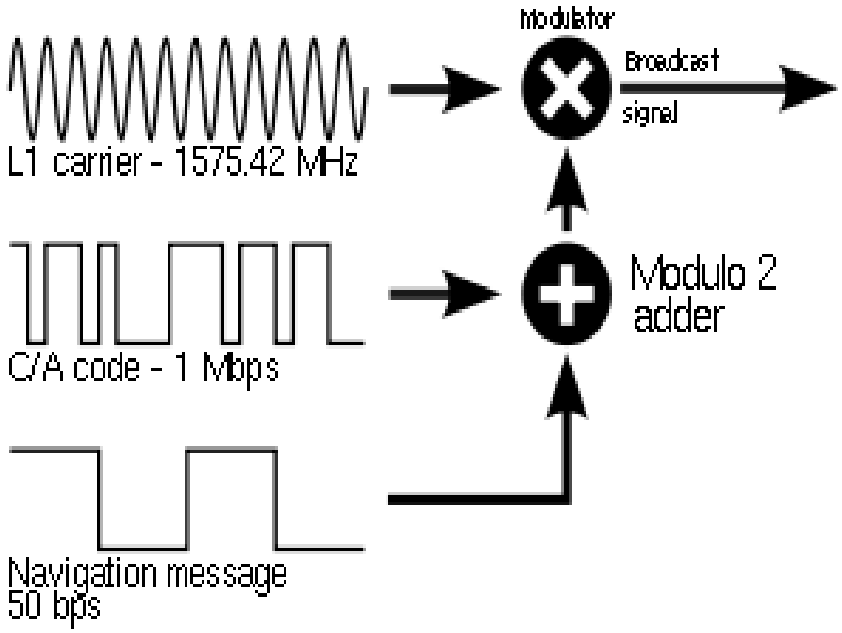

Figure 2-1 : GPS signal generation

A more detailed view can be seen in the following figure 2-2

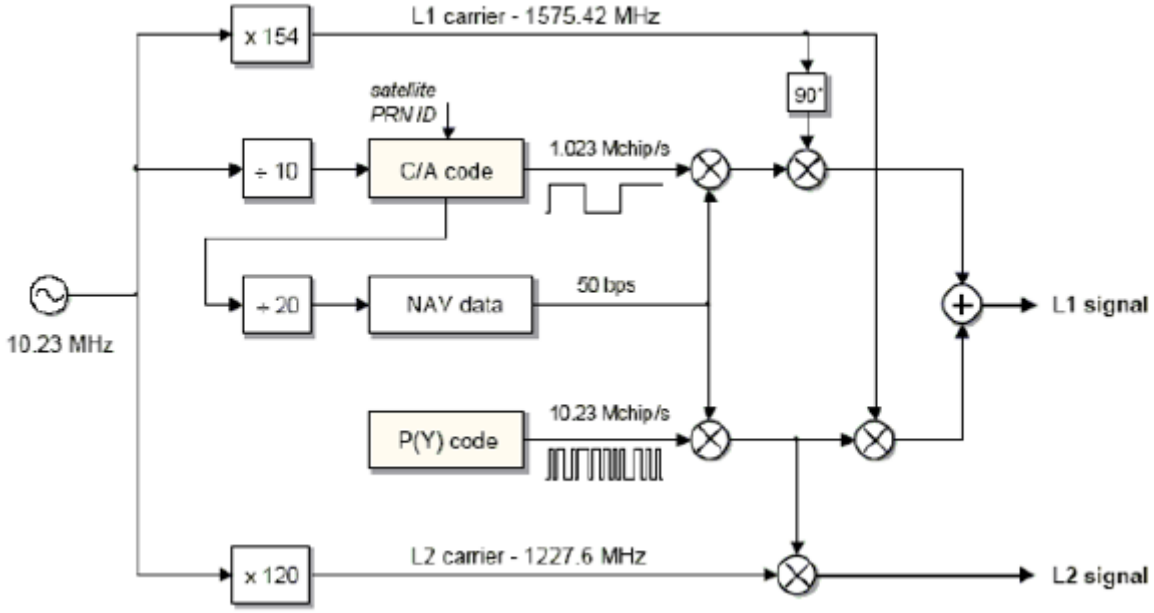

Figure 2-2 : Detailed illustration of GPS signal generation [5]

Apart from the above-mentioned codes there are other modernized and additional GPS signals as well. The modernised civilian signals are L2C, L5 and L1C. Not all satellites broadcast these signals. However, the GPS L1 band can be considered as the most important band in the field of navigation science. The spectra of L1 signals can be seen in the following figure.

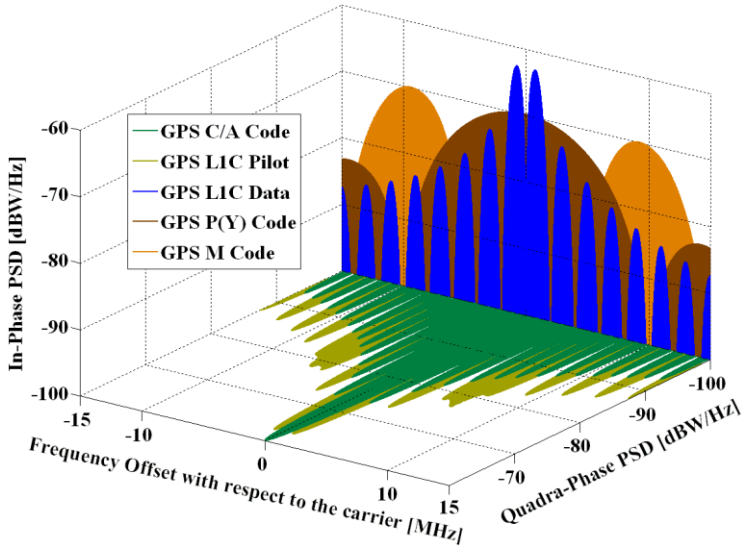

Figure 2-3 : Spectra of GPS signals in L1 [6]

The multipath analysis and estimation are performed on the logged files of GPS L1CA signals. The input available for the Multipath estimation is the dumplog files that consists of the real and imaginary parts of each of the 11 multicorrelators for both RHCP and LHCP for each PRN tracked.

2.2 SIGNAL POLARISATION

GPS signal is an EM wave characterised by its polarisation. Ideally, the signals transmitted from the GPS satellites are RHCP. A signal is RHCP if its electric field intensity (E) rotates in anti-clockwise direction and is LHCP if the E vector rotates in the clockwise direction. The circularly polarised signal can be seen as the combination of two linear polarisations. Similarly, the Electric field vector is composed of the horizontal component (E_h) and the vertical component (E_v) that are equal.

However, the polarisation of the signal changes when it gets reflected. The resulting polarisation of the signal depends upon the reflection coefficient of the reflector and the angle at which the signal reaches the reflector also known as grazing angle (θ_g). Consequently, the horizontal and vertical components of the Electric field vector are no more equal to each other because the reflecting material has a different factor of attenuation for the horizontal and the vertical components. The horizontal component always undergoes a 180-degree phase change after reflection. Whereas the phase change in the vertical component can be either 0 degrees or 180 degrees depending on whether the grazing angle is lower or greater than the Brewster angle respectively. This causes the circularly polarised signal to be elliptically polarised signal. The resulting elliptically polarised signal could be right hand polarised or left hand polarised depending on the Brewster (Ψ_B) and grazing angles (θ_g). Brewster angle also known as polarisation angle is the angle of incidence at which a signal with a certain polarisation can pass through a surface without

reflection. We can see an illustration of circular and elliptical polarisation in figures 2-4 and 2-5 respectively.

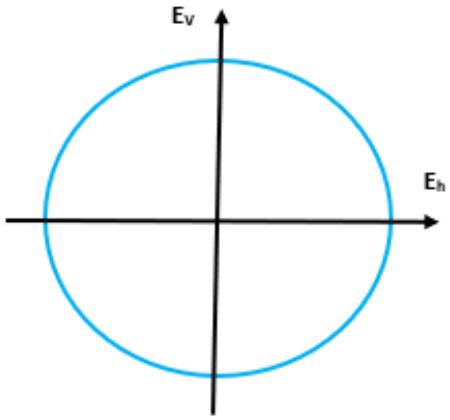

Figure 2-4 : Circular Polarisation

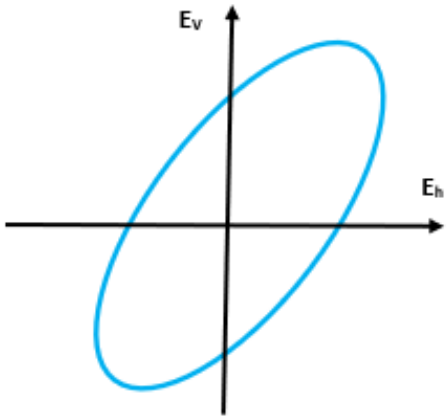

Figure 2-5 : Elliptical Polarisation

Hence, we can conclude that when the grazing angle is less than the polarisation angle the signal remains Right hand because only the horizontal component undergoes polarisation change. Alternatively, if the grazing angle is greater that the polarisation angle the resulting E vector becomes left hand polarised as a result of the change in polarity of both the horizontal and vertical components. In figure 2-6 we can better visualise the relationship between the Brewster angle and the change in polarisation of the incident wave upon reflection. In figure 2-6 we can see that when an RHCP signal incidents normally on the ground the reflected wave maintains the circular polarisation but becomes LHCP.

When the grazing angle is equal to the Brewster angle the resulting reflected signal becomes linearly polarised. When the grazing angle becomes less than the Brewster angle the wave deviates from its circular polarisation however maintaining the same direction of polarisation. When the wave has the grazing angle greater than the Brewster angle, we can see the change in the polarisation direction in the reflected signal [7].

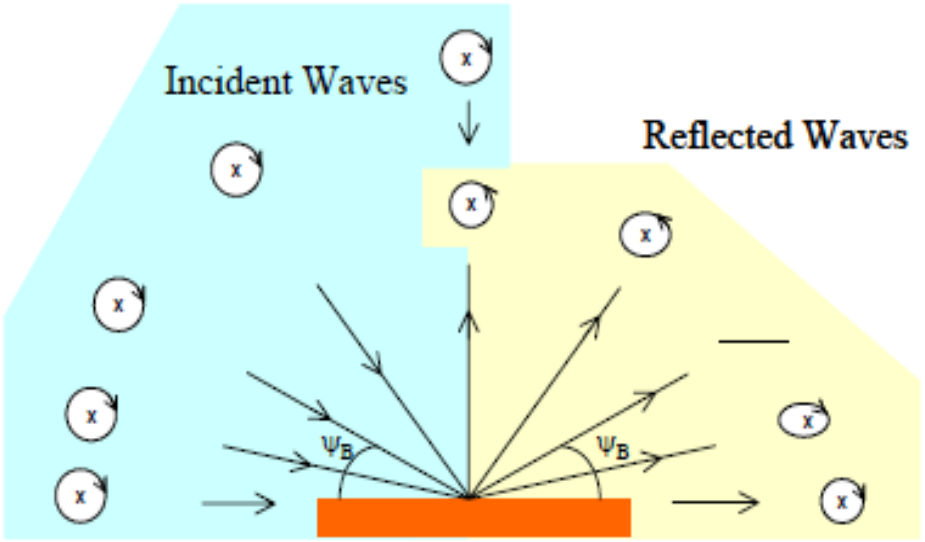

Figure 2-6 : Reflected Signal polarisation [7]

2.3 INTRODUCTION TO MULTIPATH AND ITS CHARACTERISTICS

A multipath signal is a signal that travels a longer path than the direct path after encountering some reflecting material and hence it is characterised by the parameters like relative amplitude, relative delay, relative phase, relative phase rate and relative polarisation. The relativity is with respect to the corresponding LoS signal parameters.

The Multipath amplitude depends on the reflection coefficient, shape and size of the reflecting material. The multipath signal can combine either constructively or destructively with the LoS signal depending upon the relative phase of the multipath signal. Considering the case of simple reflection, we can calculate the relative delay by using the image theory. However, to apply the image theory we assume that the signals coming from the satellites are parallel considering that the distance between the satellite and the receiving antenna is much larger than the distance between the antenna and the reflecting surface [4]. This has been illustrated in figure 2-7

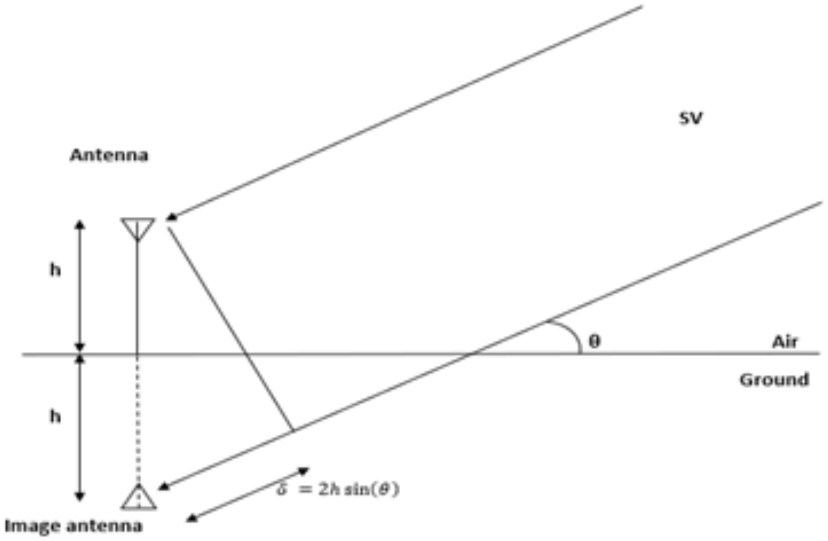

Figure 2-7 : A geometrical representation of Multipath scenario

From the figure;

Relative delay $\delta = 2 \cdot h \cdot \sin(\theta)$

The relative delay and the reflection coefficient of the material inducing the multipath determine the relative phase of the multipath signal. The multipath phase rate is given by the derivative of the relative delay. The relative phase error is calculated by taking the derivative of the relative delay. Lastly, relative polarisation of the multipath signal depends upon the reflecting surface. Typically, the GNSS signals are Right hand circularly polarised(RHCP) but upon reflection they become elliptically polarised if the reflection is caused by a non-metallic surface. Whereas the reflection from a perfectly conducting metallic surface will cause the RHCP signal to reverse its polarisation [4].

A SIMPLE SIGNAL MODEL

A composite GNSS signal model at the receiver with N-1 reflections has been shown below

$$s(t) = \sum_{i=0}^{N} a_i(t) \,.\, p(t - \tau_i(t)) \,.\, cos\big(\omega_0 t + \theta_i(t)\big) + \epsilon(t).$$

where,

$a_i(t)$	amplitude of the i[th] component
$p(t)$	GNSS signal modulation
$\tau_i(t)$	relative delay of the i[th] component
ω_0	Nominal frequency of the LoS signal
$\theta_i(t)$	relative phase of the i[th] component
$\epsilon(t)$	Noise

The LoS component corresponds to the signal when $i = 0$. The above signal model can be split into LoS and Multipath components as below

$$s_{LoS}(t) = a_0(t).p(t - \tau_0(t)).cos\big(\omega_0 t + \theta_0(t)\big) + \epsilon(t).$$

$$s_{MP}(t) = \sum_{i=1}^{N} a_i(t).p(t - \tau_i(t)).cos\big(\omega_0 t + \theta_i(t)\big) + \epsilon(t).$$

Where $s_{LoS}(t)$ and $s_{MP}(t)$ are the LoS and Multipath signal components respectively. In the thesis the case of only one reflection is studied and hence the multipath signal is

$$s_1(t) = a_1(t).p(t - \tau_1(t)).cos\big(\omega_0 t + \theta_1(t)\big) + \epsilon(t).$$

It is known that the GNSS receiver is mainly based on the calculation of correlation function between the received signal and the locally generated replica of the signal. In other words, the functionality of a navigation receiver depends on its ability to align the PRN spreading sequences used by the transmitter and the receiver. The receiver must recover the delay of the locally generated code by aligning the local code and the received code. Similarly, the carrier frequency and phase have to be recovered too. This process of synchronization is done in 2 steps namely Acquisition and Tracking.

Acquisition: The correlation between the local replica and the received signal is the basis of acquisition. In general, we can say that acquisition phase begins when the receiver starts up and ends when it detects and confirms a signal. A rough estimation of delay and Doppler shift is done

between the locally generated code and the incoming code. Hence, we can say that the core of pseudorange estimation is correlation and even a small misalignment can cause large pseudorange errors. The effect of the presence of the multipath signal on the correlation function can be seen in figure 2-8 where a simple example of a BPSK signal is shown.

Tracking: Eventually the correlation function must be processed by the receiver for tracking. Tracking follows the evolution of the signal acquired and tries to do a better alignment among the signals. It is fed with the estimated delay and doppler shift given by the acquisition stage that does a better estimation of the code delay and residual carrier frequency and phase by doing the respective procedures of carrier wipe off and code wipe off. It consists of a Phase Locked Loop (PLL) and a Delay Locked Loop (DLL). In the beginning of the tracking process code wipe off is done using the delay that was estimated in the acquisition phase of the receiver. This process of code wipe off removes the code and the subcarrier. The Phase Locked Loop (PLL) estimates the phase and frequency. After the operation of PLL it is considered that the carrier frequency and phase is removed from the signal of interest. Then a Delay Locked Loop (DLL) is implemented . A DLL discriminator uses Early (E) and Late (L) branch rather than just one prompt replica in order to perform the correlation. If the replica is well aligned with the signal, then the correlation from early and late are equal and no error can be observed.

However, the presence of multipath induces an error in the discriminator function resulting in tracking error and hence bias in pseudo range estimation. In figure 2-9 we can see this effect in the discriminator function. In the left of figure 2-9 we can see the discriminator function without multipath and on the right, we can see a discriminator function with multipath. On the right of the figure we can see that the distortion in the autocorrelation function has caused the zero crossing to shift away . This can be shown in the following figures

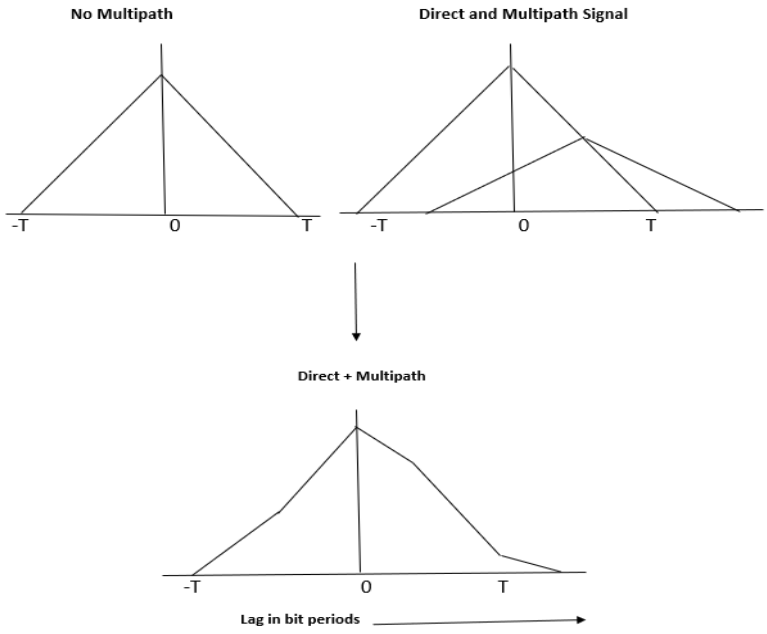

Figure 2-8 Combined correlation function for the direct and multipath signal

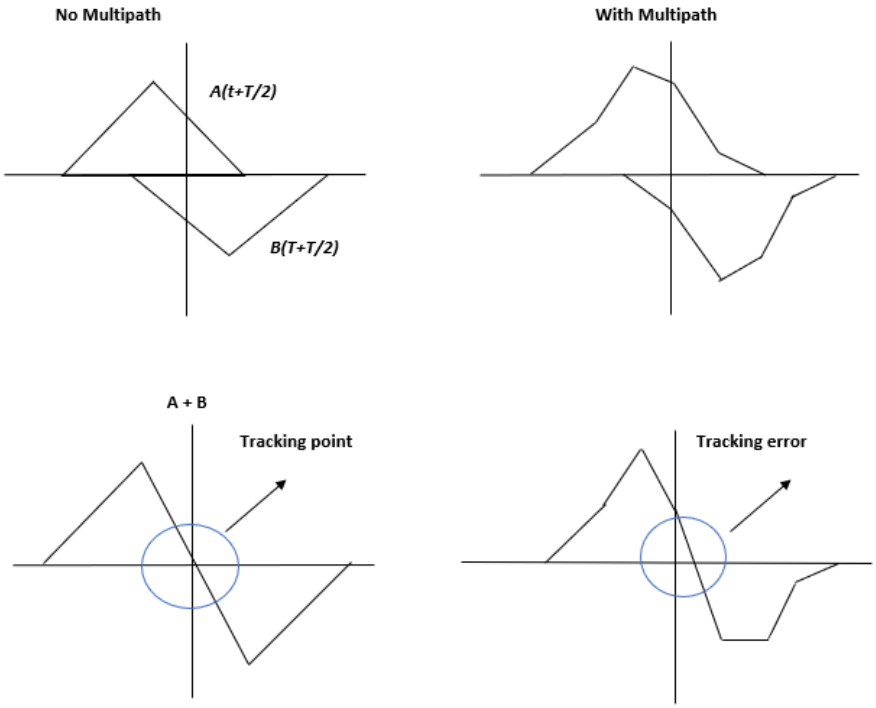

Figure 2-9 : Discriminator function without multipath and in the presence of multipath

The error caused due to the multipath presence can be measured with the help of Multipath Error Envelope (MEE). It is a graphical illustration of the tracking error with respect to the relative delay. In the figure presented in 2-10 we can see that the MEE can be divided in two parts the positive and the negative tracking error respectively.

Interference due to multipath can be called as constructive if it has a phase of zero degrees and destructive if it has the phase of 180 degrees and this bound is represented in the error envelope in figure 2-10. In this figure we can see the error envelope considering a single multipath signal having an amplitude half to that of the direct signal and 1 chip early to late spacing.

The upper half of the envelope represents the case of maximum error in which the multipath signal is in-phase (0°) with the LoS signal. Consequently, the lower half of the envelope represents the case of minimum error in which the multipath signal is out of phase (180°) with respect to the LoS signal. The error in pseudorange for all other phases will lie within this minimum-maximum envelope. A simplified error envelope corresponding to a specular reflection scenario can be seen in the following figure [4].

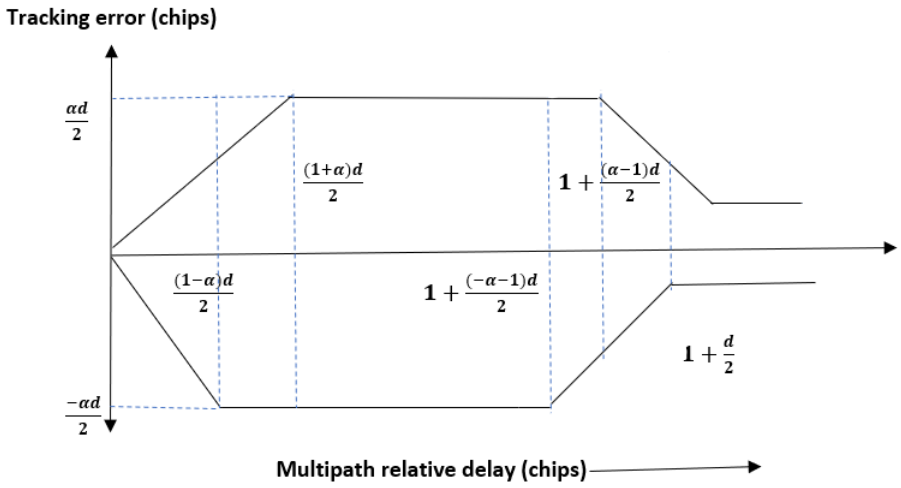

Figure 2-10 : Multipath Error Envelope

In the figure α refers to the ratio between the amplitudes of the multipath to the direct signal, d refers to the spacing between the early and late correlators and the maximum and minimum pseudorange error are given by $\frac{\alpha d}{2}$ and $\frac{-\alpha d}{2}$ respectively [4].

The figure shows the relation between the relative delay and the minimum-maximum possible errors. We can see that the maximum positive error occurs at larger relative delay than the maximum negative error. In the figure we can see that as the relative delay gets larger the error envelope doesn't converge to zero due to the presence of sidelobes in the autocorrelation function calculation. The above error envelope corresponds to the simple BPSK(1) however this general multipath error envelope binds all other error envelopes for signals using modern modulations like Binary Offset Carrier (BOC), Multiplexed Binary Offset Carrier (MBOC) or Composite Binary Offset Carrier (CBOC). BOC modulation is generated by using squared subcarrier to the conventional BPSK. It is usually denoted as BOC(n,m) where n refers to the subcarrier frequency that is in the multiples of 1.023 Mega Hertz (MHz) and m refers to the chip rate in the multiples of 1.023 Mega Chips (Mcps). MBOC was implemented as a modernization for the BOC signals. In these signals in order to improve the tracking efficiency a slight amount of additional power at higher frequency is placed. For example, in Time Multiplexed BOC (TMBOC), BOC(6,1) and BOC(1,1) are combined and in Composite BOC (CBOC), BOC(6,1) is transmitted in time division. Both CBOC and TMBOC are the categories of MBOC [8].

3 LITERATURE REVIEW FOR MULTIPATH ESTIMATION TECHNIQUES

Given the spread spectrum nature of GNSS signals they are robust towards interference due to the reflected signals received with the delay of greater than 1 chip, but the problem arises due to the reception of the reflected signals with delay lower than 1 chip period [4]. Hence multipath mitigation is a must especially in these scenarios to ensure accurate positioning. Various multipath estimation and mitigation techniques have been studied and analysed in the literature and in this section, we reassume those techniques for multipath mitigation. This section wants to introduce some techniques which can be useful also for multipath parameter estimation. Some of these techniques make use of special antennas like choke ring to limit multipath , some use post processing methods to mitigate the effect of multipath while some use correlation-based techniques.

3.1 MULTIPATH MITIGATION TECHNIQUES AT ANTENNA LEVEL

As trivial as it may sound but the best way to mitigate multipath is to stay away from it i.e. position the antenna in an environment where there is very low multipath presence. Apart from this, the choice of antenna can play a major role in multipath mitigation. We may choose an antenna that preserves our desired LoS signal strength while attenuating the multipath component.

3.1.1 Single element antenna

It refers to the antennas that are put on special ground planes with RF absorber designed to reduce the effect of multipath. However, this method was not used so much because of the material cost and the effect of weather conditions on it. After this, choke ring antenna was developed and widely accepted as a multipath reducing technique that includes a single antenna placed in a base

that consists of conductive rings with the same centre. This design was able to effectively choke out the EM waves that arrive at a very low or negative elevation angles. Despite being a very popular technique the problem with this method is its non-portability.

3.1.2 Phased array antenna

This technique was introduced as the result of the need to provide a better gain and hence a better availability even in low elevation angles at 5° that the above techniques cannot address. For example, the first among them to be introduced consisted of multiple element linearly polarised dipole antennas placed vertically in a stack in combination with one circularly polarised antenna component placed on a concave reflecting object. The second type of this design consists of circularly polarised antenna elements placed vertically on top of each other. The advantage of this design compared to the first design is its simplicity in hardware because of the use of a single receiver instead of two and simple software implementation [4].

3.2 RECEIVER CORRELATOR BASED TECHNIQUES FOR MULTIPATH MITIGATION

The most common technique under this category is the use of narrow correlators (NC). This involves reducing the spacing between the Early and the Late correlators of the traditional Delay Locked Loop (DLL). The correlator spacing depends on the front-end bandwidth available in the receiver. The most typical spacing used is of 0.1 chips. This reduction results in more accurate pseudorange estimation as well as significantly reduces the multipath error. This technique reduces the long delay multipath significantly however, the multipath due to short delay is not compensated by it. This method is not very suitable for the mass market applications because of its hardware complexity because of the use of large IF Bandwidth.

Another technique that works at the correlation level is the Double Delta method that uses five correlators instead of conventional three correlators. The NC is mostly used in the low-cost narrow-band receivers built in an economic way, whereas the Double Delta method is used in a wide-band receiver. Strobe correlator also works using double delta discriminator. Multipath Elimination Technology (MET) and Pulse Aperture Correlator (PAC) also uses this concept of two additional arms [9]. This concept can be extended with more correlators (for e.g. 10-15)spaced at small intervals for better multipath mitigation

3.3 MULTIPATH PARAMETERS ESTIMATION USING MULTI-CORRELATORS AND LEAST SQUARES METHOD

This method is based on the use of Least Squares (LS) technique to estimate various multipath parameters by processing the multicorrelator outputs. It focuses on improving the tracking loops performance by removing the multipath parameters. The receiver is based on a multicorrelator architecture which means that the incoming signal correlates with several replicas of the locally generated code. This method performs multipath parameters estimation using a recursive LS method , hence a mathematical model of the signal is built and aimed to reduce the Euclidian distance between the real measurements and the model. This method was proven to estimate various multipath parameters like relative amplitude, delay and phase with a fine and consistent accuracy for multipath delays that are greater than 0.06 chip [10].

3.4 MULTIPATH ESTIMATION AND MITIGATION VIA POLARISATION SENSING DIVERSITY

This technique is based on the principle of strengthening the unwanted multipath signals in order to ease their estimation and finally remove them. It exploits the polarisation sensing diversity

of the DPA, dual coherent RF frontend and a signal processor that works with the master-slave principle. The availability of correlation functions for both the received RHCP and LHCP signals helps in Parallel Iterative Cross Cancelation (PICC) of direct and Multipath signals in the RHCP and LHCP correlations ultimately facilitating multipath mitigation. After various iterations the RHCP signals become free of multipath that allows the estimation of LoS signal. Finally, this estimated LoS signal can be removed from the LHCP signal which leaves only the Multipath signal [7].

3.5 MULTIPATH PARAMETERS ESTIMATION USING EKF AND DUAL RHCP/LHCP ANTENNA

As the name suggests this method uses Kalman Filter for multipath parameters estimation by processing the data obtained from a RHCP and LHCP chains of a Dual Polarized Antenna (DPA). The Kalman Multipath (KMP) algorithm for the estimation of multipath parameters is introduced and described in detail [11]. It uses the data from a Dual Polarised antenna in order to evaluate and characterize the multipath environment and the errors in pseudorange caused by it. The estimated multipath parameters using the observations from both the RHCP and LHCP antenna were used to analyse the effect of the polarisation of the antenna on the composite signals received.

In the frame of this thesis work we analysed the EKF technique for multipath parameter estimation, working with multi-correlators observables coming from the RHCP and LHCP. Hence, we used a diversity gain due to antenna in dual polarisation and multicorrelator diversity. Here the use of DPA is an added value because more information is provided by the Left multi-correlators . The RHCP and LHCP signal and model has common parameters together so there are lesser parameters to be estimated and there is a gain in using the left part at the cost of complexity, double

the hardware and processing. The antenna shall be properly selected in order to provide LHCP antenna gain higher for lower elevation in order to increase the sensitivity to multipath reflection.

In the next chapter, the signal model useful for EKF scheme design will be described, considering the availability of multi-correlators values at post-correlation level and the High Sensitivity Receiver configuration (RHCP and LHCP tracking).

4 MULTIPATH SIGNAL MODEL

The work performed in the thesis involves the processing of the composite signals received using both the RHCP and LHCP chains. Hence, signals from both the chains need to be modelled which is illustrated in this chapter. A simple case of single reflection is taken where the model consists of a LoS signal and a delayed version of the direct signal superimposed together.

4.1 SIGNAL MODELLING

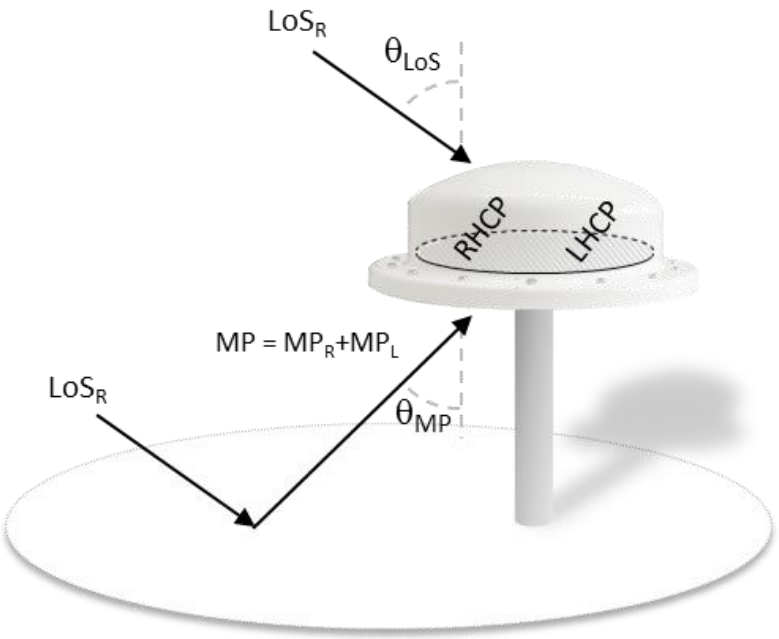

Figure 4-1 : A simple Multipath scenario [1]

In the figure above we can see that the receiver consists of RHCP and LHCP processing chains. It shows the reception of the LoS and Multipath signal at RHCP antenna and the illustration is similar in case of LHCP antenna as well. The LoS_R signal is received by the antenna at an angle of θ_{LoS}. We can see that another LoS signal, LoS_R, reflected on the ground has reached the antenna

at an angle θ_{MP}. As discussed in the previous chapter ,the GPS signal, which is originally RHCP when reflected has become elliptically polarised and is a combination of RHCP and LHCP multipath terms.

4.1.1 RHCP Chain

The RHCP chain consists of RHCP antenna outputs and RHCP receiver processing chain. The multipath signal will be received in the RHCP antenna as the combination of RHCP and LHCP signals. As stated, before a case of single reflection is considered.

$$r_R(t) = LoS_1 + MP_{\mathrm{R}} + MP_{\mathrm{L}}$$

$$r_R(t) = G_R(\theta_{\mathrm{LoS}}) \cdot LoS_1 + G_R(\theta_{\mathrm{MP}}) \cdot LoS_2 + G_{XR}(\theta_{\mathrm{MP}}) \cdot LoS_2$$

The RHCP LoS signal and the RHCP multipath component are the major signal contributions seen on the RHCP side because of co-polar signal amplification. Whereas, the LHCP multipath component will have a very low contribution because it will be attenuated by the cross-polar gain of the RHCP antenna. The LoS signal is received with an angle of θ_{LoS} and the reflected signal is received with an angle of θ_{MP}.

The received signal considering the relationship between the antenna coefficients and the angles of reception can be written as :

$$r_R(t) = G_R(\theta_{\mathrm{LoS}}) \cdot s(t - \tau_0) + \Gamma \cdot C \cdot G_R(\theta_{\mathrm{MP}}) \cdot s(t - \tau_0 - \tau_{MP}) + \Gamma \cdot (1 - C) \cdot G_{XR}(\theta_{\mathrm{MP}}) \cdot s(t - \tau_0 - \tau_{MP})$$

Where,

$r_R(t)$	Received composite signal
τ_0	The code delay of LoS signal
τ_{MP}	The code delay of the multipath signal

s	The transmitted signal
Γ	reflection coefficient
C	a factor that shows the percentage of RHCP power as a function of total multipath power
G_R	Co-polar gain
G_{XR}	Cross polar gain
θ_{LoS}	Angle of reception of LoS signal
θ_{MP}	Angle of reception of the multipath signal

$$r_R(t) = G_R(\theta_{\mathrm{LoS}}) \cdot s(t-\tau_0) + (\Gamma \cdot C \cdot G_R(\theta_{\mathrm{MP}}) + \Gamma \cdot (1-C) \cdot G_{XR}(\theta_{\mathrm{MP}})) \cdot s(t-\tau_0-\tau_{MP})$$

The antenna gains for RHCP and LHCP multipath components and reflection coefficient can be denoted by χ_R i.e.

$$\chi_R = \Gamma \cdot C \cdot G_R(\theta_{\mathrm{MP}}) + \Gamma \cdot (1-C) \cdot G_{XR}(\theta_{\mathrm{MP}}) = |\chi_R| e^{j\angle x_R}$$

$$r_R(t) = G_R(\theta_{\mathrm{LoS}}) \cdot s(t-\tau_0) + \chi_R \cdot s(t-\tau_0-\tau_{MP})$$

Where,

$$s(t-\tau_0) = \sqrt{2 \cdot P} \cdot d \cdot \cos(2\pi f t + \theta_0) \cdot c(t-\tau_0)$$

$$s(t-\tau_0-\tau_{MP}) = \sqrt{2 \cdot P} \cdot d \cdot \cos(2\pi f t + \theta_1) \cdot c(t-\tau_0-\tau_{MP})$$

The received signal then can be represented by :

$$r_R(t) = G_R(\theta_{\mathrm{LoS}}) \cdot \sqrt{2 \cdot P} \cdot d \cdot \cos(2\pi f t + \theta_0) \cdot c(t-\tau_0) + \chi_R \cdot \sqrt{2 \cdot P} \cdot d \cdot \cos(2\pi f t + \theta_1) \cdot c(t-\tau_0-\tau_{MP})$$

Where,

P	signal power
d	navigation bit
f	GPS signal carrier frequency
c	C/A code sequence
τ_0	Code delay for the LoS signal
τ_{MP}	Code delay for the Multipath signal
θ_1	carrier phase for the signal 2 relative to the LOS signal

The multipath signal goes through an extra path length before reaching the receiver adding some more delay τ_{MP}''. We include all the delays for the multipath signal by a single delay term τ_1. The reflection coefficient of the reflecting material introduces some changes in the phase and amplitude of the receiving signal. The RHCP antenna itself also introduces some carrier phase changes.

We can write the received signal as:

$$r_R(t) = G_R(\theta_{\text{LoS}}) \cdot \sqrt{2 \cdot P} \cdot d \cdot \cos(2\pi f t + \theta_0 + \theta_R) \cdot c(t - \tau_0) + \quad |\chi_R| \cdot \sqrt{2 \cdot P} \cdot d \cdot \cos(2\pi f t + \theta_1 + \angle\chi_R) \cdot c(t - \tau_0 - \tau_1)$$

Simplifying further,

$$\theta_{LoS}{}^{RR} = \theta_0 + \theta_R \qquad \alpha_{LOS}^{RR} = G_R(\theta_{\text{LoS}}) \cdot \sqrt{2 \cdot P}$$

$$\theta_{MP}{}^{R} = \theta_1 + \angle\chi_R \qquad \alpha_{MP}^{R} = |\chi_R| \cdot \sqrt{2 \cdot P}$$

The received signal can be finally written as :

$$r_R(t) = \alpha_{LoS}^{RR} \cdot \sqrt{2 \cdot P} \cdot d \cdot \cos(2\pi f t + \theta_{LoS}{}^{RR}) \cdot c(t - \tau_0) + \quad \alpha_{MP}^{R} \cdot d \cdot \cos(2\pi f t + \theta_{MP}{}^{R}) \cdot c(t - \tau_0 - \tau_1)$$

The received signal $r_R(t)$ is then correlated with the locally generated signals at the receiver multicorrelators. The received used to acquire the signals analysed in the thesis has 11 multicorrelators equally spaced at 0.05115 chips.

The local signal is generated for both RHCP and LHCP tracking chains:

$$Local(t) = L_{Local} \cdot d \cdot \cos(2\pi f_{Local} t + \theta_{Local}) \cdot c(t - \tau_{Local})$$

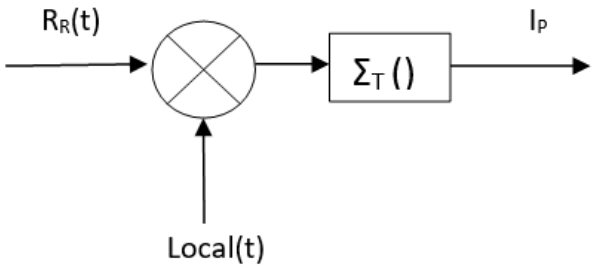

Figure 4-2 : Correlation between incoming signal and the local signal

The correlator output can be written as:

$$I_{\Delta m} = d \cdot \alpha_{LoS}^{RR} \cdot sinc(\delta f T) \cdot R(\delta\tau_{LoS}^{R} + \Delta m) \cdot \cos(\delta\phi_{\mathrm{LoS}}^{RR}) + d \cdot \alpha_{MP}^{R} \cdot sinc(\delta f T) \cdot R(\delta\tau_{LoS}^{R} - \delta\tau_{MP}^{R} + \Delta m) \cdot \cos\left(\delta\phi_{Mp}^{R}\right)$$

$$Q_{\Delta m} = d \cdot \alpha_{LoS}^{RR} \cdot sinc(\delta f T) \cdot R(\delta\tau_{LoS}^{R} + \Delta m) \cdot sin(\delta\phi_{\mathrm{cos}}^{RR}) + d \cdot \alpha_{MP}^{R} \cdot sinc(\delta f T) \cdot R(\delta\tau_{LoS}^{R} - \delta\tau_{MP}^{R} + \Delta m) \cdot \sin\left(\delta\phi_{Mp}^{R}\right)$$

A code wipe off operation is performed in the algorithm, so the data bits are disregarded from the model .The sinc terms have been removed too considering it constant and combined with the amplitude .

For making the equations simple a complex exponential representation of the above equations as the combination of In-phase and Quad-phase terms is done. The signal model can be represented as given below.

$$(\boldsymbol{I_{\Delta m} + jQ_{\Delta m}})_{\boldsymbol{R}} = \boldsymbol{\alpha_{LoS}^{RR}} \cdot \boldsymbol{R}\left(\boldsymbol{\delta\tau_{LoS}^{R} + \Delta m}\right) \cdot \boldsymbol{e^{j(\delta\phi_{\mathrm{LOS}}^{RR})}} + \boldsymbol{\alpha_{MP}^{R}} \cdot \boldsymbol{R}\left(\boldsymbol{\delta\tau_{LoS}^{R} - \delta\tau_{MP}^{R} + \Delta m}\right) \cdot \boldsymbol{e^{j(\delta\phi_{\mathrm{MP}}^{R})}}$$

Where,

α_{LoS}^{RR}	LOS signal amplitude at RHCP
$\delta\phi_{\mathrm{LoS}}^{RR}$	Average phase error for the LOS signal
α_{MP}^{R}	RHCP multipath amplitude
$\delta\phi_{\mathrm{MP}}^{R}$	Average phase error for the RHCP Multipath signal
$\delta\tau_{LoS}^{R}$	The difference between the tracked pseudorange at RHCP and actual pseudo range($\tau_{LOS}^{'} - \tau_{LOS}^{R}$)
$\tau_{LOS}^{'}$	The measured LoS delay taken from the database at the RHCP chain
τ_{LoS}^{R}	The actual LoS delay .
$\delta\tau_{MP}^{R}$	The relative multipath tracking error at RHCP which is considered the same for LHCP and for both the multipath components.

4.1.2 LHCP Chain

The LHCP chain consists of LHCP antenna outputs and LHCP receiver processing chain. The multipath signal model at LHCP after performing the similar steps as in the RHCP chain can be seen as below:

$$(\boldsymbol{I_{\Delta m} + jQ_{\Delta m}})_L = \boldsymbol{\alpha_{LoS}^{LR}}.\boldsymbol{R}\big(\epsilon + \boldsymbol{\delta\tau_{LoS}^{R}} + \boldsymbol{\Delta m}\big).\boldsymbol{e}^{j(\delta\phi_{\mathrm{LoS}}^{LR})} + \boldsymbol{\alpha_{MP}^{L}} \cdot \boldsymbol{R}\big(\epsilon + \boldsymbol{\delta\tau_{LoS}^{R}} - \boldsymbol{\delta\tau_{MP}^{R}} + \boldsymbol{\Delta m}\big).\boldsymbol{e}^{j(\delta\phi_{\mathrm{MP}}^{L})}$$

Where,

α_{LoS}^{LR}	Right Hand Polarised LoS signal amplitude at LHCP
$\delta\phi_{\mathrm{LoS}}^{LR}$	Average phase error for the LoS signal
α_{MP}^{L}	LHCP multipath amplitude
$\delta\phi_{\mathrm{MP}}^{L}$	Average phase error for the LHCP Multipath signal
ϵ	Difference between the tracked pseudo range in LHCP chain and RHCP chain(from the database). $\epsilon = (\tau_{LoS}^{''} - \tau_{LoS}^{'})$
$\tau_{LoS}^{''}$	The measured LoS delay taken from the database at the LHCP chain

It is worth to remember that two possible architectures for RHCP and LHCP tracking's can be considered which are briefly explained below.

- **Slaved Architecture :** The receiver used in the work consists of a DPA and hence it has two separate RF channels to process the signals received in the RHCP and LHCP antenna components. In this architecture the one chain among the two functions as the Master and the other chain functions as the slave. One tracking channel is required for a satellite and the code and carrier loops get locked with the signal from the RHCP antenna. The second channel also called as slave uses the same code and carrier replicas and lags that are used by the master to process the incoming LHCP signal [7].
- **Not slaved architecture:** In this architecture there is no master and slave and each chain uses an independent code and carrier replica Hence, the processing of the RHCP and LHCP chain is independent.

In the frame of this work, the receiver is configured to have LHCP tracking not slaved with respect to RHCP, so the two tracking are independent and the ϵ must be modelled and can be hypothesized equal to pseudorange difference measurements available from the receiver.

4.2 RELATIONSHIP BETWEEN RHCP AND LHCP MODELS

The following figure represents a general geometry of a simplified multipath model resulting from both Line of Sight (LoS) signal and its corresponding first reflection echo. This simple figure also shows the relationship between the RHCP and LHCP models that are assumed in this work.

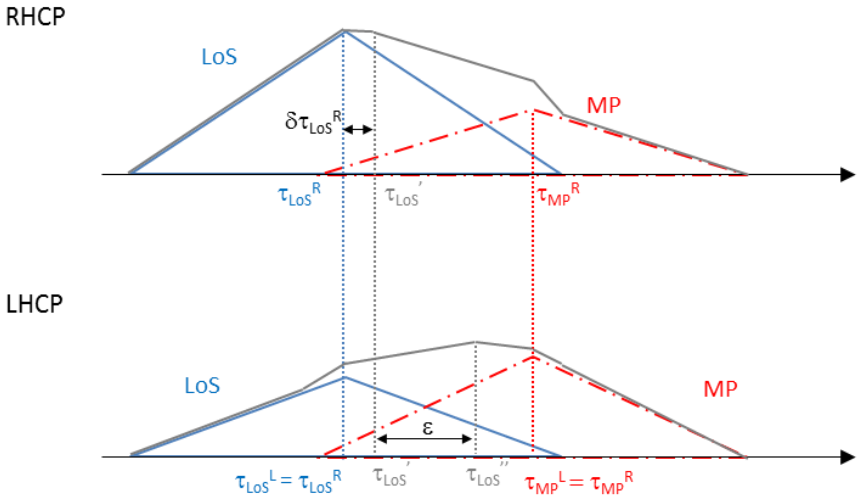

Figure 4-3 : Multipath Reflection Model [1]

From the above figure we can see that the actual Line of Sight delay at the RHCP and LHCP is considered as the same ($\tau_{LoS}^{R} = \tau_{LoS}^{L}$). Similarly, another common parameter in the two models is the multipath delay which is considered equal as well ($\tau_{MP}^{R} = \tau_{MP}^{L}$).

In this simplification, approximation is only in terms of group delay which can be different from RHCP and LHCP physical chains. This is valid in first approximation considering that the parameters to be estimated are well larger than the group delay differences.

5 REVIEW OF THE EKF TECHNIQUES

This chapter gives a detailed account of the techniques used to estimate the multipath parameters. The I and Q multicorrelators samples are fed into the Extended Kalman Filter (EKF) which in turn estimates the multipath parameters. In this chapter the basic theory of the conventional Kalman Filter and its enhanced version EKF is well explained. In addition to this a detailed description of the constrained version of the EKF is done. The results generated from both the conventional EKF and constrained EKF are presented in the next chapters. Apart from the description on Kalman filters the states to be estimated and their formulated models are reported in this chapter.

5.1 KALMAN FILTER THEORY

Kalman Filter is a very popular and optimal linear estimator that uses measurements taken over time with white noise to estimate states. The very basic principle of Kalman Filter just like any other filter is to provide an optimal estimate of the systems state when given a data from the noisy environment. It is a recursive filter that provides the state estimates by using the estimated states of the previous time instant and the current measurements. This algorithm has been very important in the field of navigation science, guidance, aircraft and vehicle control, signal processing etc. It is also used as a very common data and sensor fusion algorithm. This algorithm uses the models of the state called as plant models and model of the measurement dynamics called as observation models to estimate the states. This iterative algorithm works in two steps prediction and correction.

The steps of the Kalman filter can be shown below.

- **Step 1 – Building a Model**

The plant and measurement models of a system can be written as below:

$$x_k = Fx_{k-1} + w_{k-1}$$

$$z_k = H_k x_k + v_k$$

x_k is the vector of states that needs to be estimated. It is the linear combination of the state transition matrix (F) and the previous estimated state(x_{k-1}) plus the process noise w_{k-1}.

z_k is the measurement vector which is the linear combination of the observation matrix (H_k), the state vector(x_k) and the measurement noise (v_k).

The process and the measurement noise are assumed to be uncorrelated, zero mean and Gaussian processes given by:

$$E\{w_k\} = 0$$

$$E\{w_k w_j^T\} = \delta(k-j)Q_k$$

And

$$E\{v_k\} = 0$$

$$E\{v_k v_j^T\} = \delta(k-j)R_k$$

$$E\{v_k w_j^T\} = 0$$

Where $\delta(k-j)$ is the Kronecker delta Function.

- **Step 2 : Prediction**

The a priori state vector estimates at time instant($\hat{x}_{k|k-1}$) is computed using the state transition matrix (F) and the previous state estimate($\hat{x}_{k-1|k-1}$). In case of the first iteration of the filter the previous state estimate is taken as the initial values that the state vector is initialised to.

$$\hat{x}_{k|k-1} = F \cdot \hat{x}_{k-1|k-1}$$

The a priori covariance matrix at time instant k is computed using the state transition matrix (F), the previous covariance matrix estimate($P_{k-1|k-1}$) and the process error covariance matrix (Q_{k-1})

$$P_{k|k-1} = F \cdot P_{k-1|k-1} \cdot F^{\top} + Q_{k-1}$$

- **Step 3 : Correction**

The Kalman gain at time instant k is calculated using the covariance matrix from the step 2 ($P_{k|k-1}$), the observation matrix (H_k), and the measurement noise covariance matrix (R_k)

$$K_k = P_{k|k-1} \cdot H_k^T \left(H_k \cdot P_{k|k-1} \cdot H_k^T + R_k\right)^{-1}$$

The posteriori covariance matrix at time instant k can be calculated as given below:

$$P_k = (I - k_k H_k) P_{k|k-1}$$

The posteriori state estimate at instant k can be calculated as given below:

$$\hat{x}_{k|k} = \hat{x}_{k|k-1} + K_k\left(Z_k - H_k \cdot \hat{x}_{k|k-1}\right)$$

Where Z_k is the measurement vector at the time instant k.

5.2 EXTENDED KALMAN FILTER

Extended Kalman Filter (EKF) is the **nonlinear version** of the conventional Kalman Filter that we discussed above. The steps are almost the same with few modifications. The plant and measurement models in many of today's applications are nonlinear and there is a nonlinear relationship between the states of the system and system dynamics and measurements. Extended Kalman filter works by transforming the nonlinear models at each time instant into linearized systems of equations. This linearization process makes the system sub optimal. The optimality of the EKF depends upon the models of the states and the initialisations made. The steps for Extended Kalman Filter can be shown as:

- **Step 1 – Building a Model**

The plant and measurement models of a system can be written as below:

$$x_k = f(x_{k-1}) + w_{k-1}$$

$$z_k = h_k(x_k) + v_k$$

x_k is the vector of states that needs to be estimated. It is related to the previous estimated state(x_{k-1}) by the non linear function f plus the process noise w_{k-1}.

z_k is the measurement vector related to the state vector(x_k) by the nonlinear function h plus the measurement noise (v_k). f and h are the nonlinear functions that are differentiable at the state vector.

Linearization of these nonlinear functions is a step that makes EKF different than the conventional Kalman Filter.

The process and the measurement noise are assumed to be uncorrelated, zero mean and gaussian processes given by:

$$E\{w_k\} = 0$$

$$E\{w_k w_j^T\} = \delta(k-j)Q_k$$

and

$$E\{v_k\} = 0$$

$$E\{v_k v_j^T\} = \delta(k-j)R_k$$

$$E\{v_k w_j^T\} = 0$$

Where $\delta(k-j)$ is the Kronecker delta Function.

- **Step 2 : Prediction**

The a priori state estimates at the current time k ($\hat{x}_{k|k-1}$) is computed using the function f and the previous state estimate($\hat{x}_{k-1|k-1}$). In case of the first iteration of the filter the previous state estimate is taken as the initial values that the state vector is initialised to

$$\hat{x}_{k|k-1} = f \cdot \hat{x}_{k-1|k-1}$$

EKF works using the innovation which is the difference between the real current measurement and the predicted measurement. It can be computed as:

$$\hat{Z}_k = h_k(\hat{x}_{k-1|k-1})$$

The nonlinear function f is linearized around the states estimates of the previous time instant. This is done taking the Jacobian of the state transition matrix.

$$F_{k-1} = \left[\frac{\partial f}{\partial x}\right]_{x=x_{k-1|k-1}}$$

Similarly, the nonlinear function h is linearized around the predicted state estimate. The linearization is done using the Jacobian here too.

$$H_k = \left[\frac{\partial h}{\partial x}\right]_{x=x_{k|k-1}}$$

The a priori covariance matrix at the current time instant i.e. k is computed using the linearized state transition matrix (F), the previous covariance matrix estimate($P_{k-1|k-1}$) and the process error covariance matrix(Q_{k-1}).

$$P_{k|k-1} = F \cdot P_{k-1|k-1} \cdot F^{\top} + Q_{k-1}$$

- **Step 3 : Correction**

The measurements are obtained as the update step requires the calculation of innovation. The Kalman gain at time instant k is calculated using the covariance matrix from the step 2($P_{k|k-1}$), the linearized observation matrix (H_k), and the measurement noise covariance matrix (R_k).

$$K_k = P_{k|k-1} \cdot H_k^T \left(H_k \cdot P_{k|k-1} \cdot H_k^T + R_k\right)^{-1}$$

The posteriori covariance matrix at time instant k can be calculated as given below:

$$P_k = (I - k_k H_k) P_{k|k-1}$$

The posteriori state estimate at instant k can be calculated as given below:

$$\hat{x}_{k|k} = \hat{x}_{k|k-1} + K_k\left(Z_k - \hat{Z}_k\right)$$

Where Z_k is the measurement vector at the time instant k and $\hat{Z}_k$ is the predicted measurement calculated in step 1.

5.3 OBSERVABLES PRELIMINARY VIEW

The signals analysed in the thesis are GPS L1CA received using both the RHCP and LHCP chains. Since the receiver had 11 multi-correlators spaced equally, the received signal comprises of I and Q samples from all the 11 correlators for both the chains.

The signals from RHCP and LHCP chains for GPS SV-31 as given below:

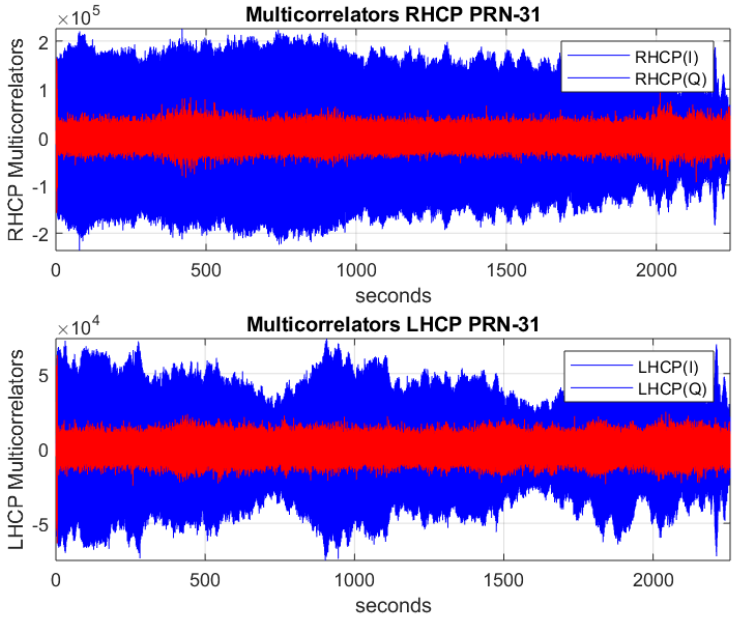

Figure 5-1 : RHCP and LHCP multicorrelators observable

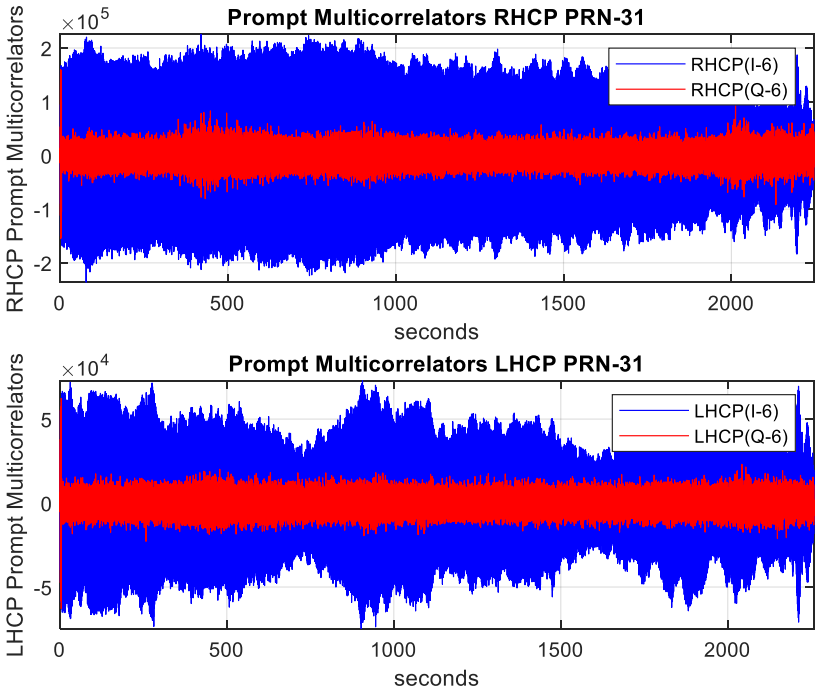

Figure 5-2 : RHCP and LHCP prompt correlators

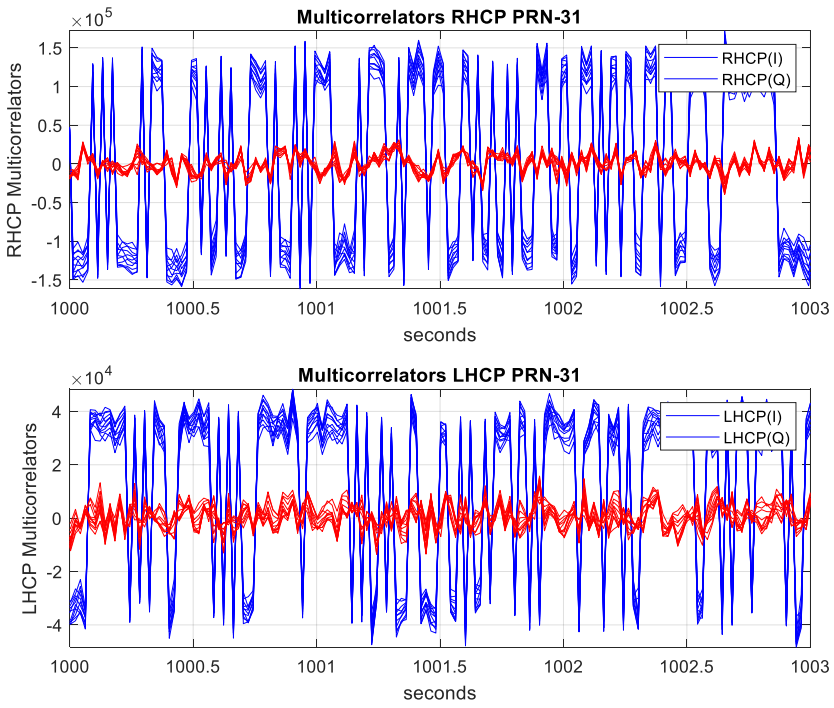

Figure 5-3 : RHCP and LHCP multicorrelators for a short interval

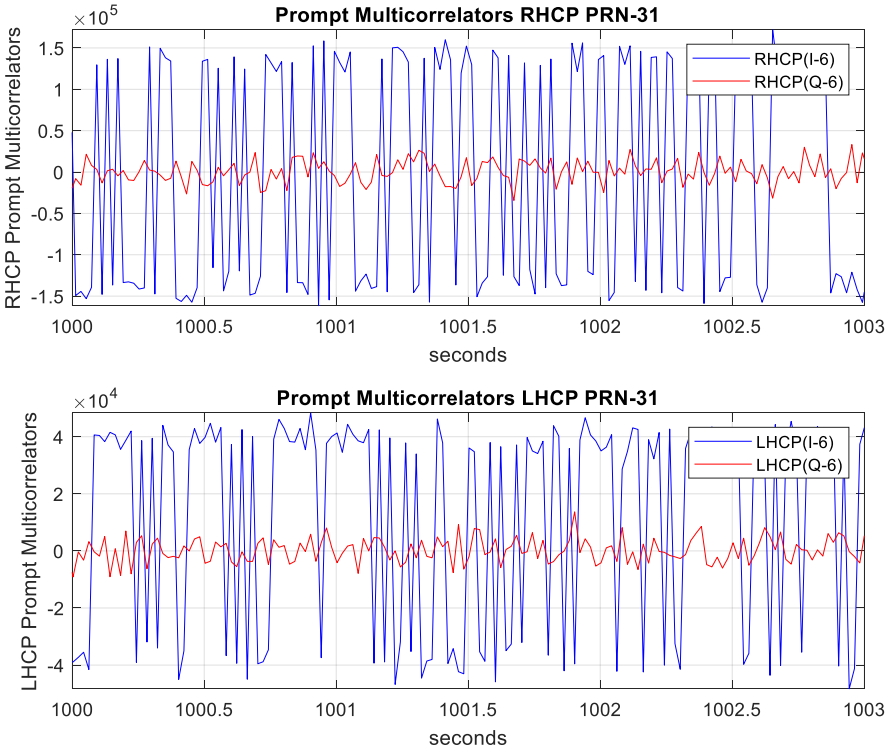

Figure 5-4 : RHCP and LHCP prompt multicorrelator for short interval

From the above it can be seen that most of the signal power is in the In phase (I) component of the signal and the Quadrature (Q) component of the signal is almost always around zero. It must be noted that only the valid measurements have been considered for the analysis. The unnecessary outliers in both the I and Q observables for both the RHCP and LHCP chains have been removed, the time axis for both the chains well aligned to ease the estimation process. Apart from this also the presence of valid pseudorange entries have been considered.

The measured C/No is one of the important entries in the database in order to understand the possible presence of the multipath in the signal especially at lower elevation: In fact, the difference between the C/No in the RHCP and LHCP chain can be used as a technique for multipath detection.

This technique has been used in [12] to distinguish between the low multipath, medium and high multipath environment.

In the case of our database for PRN-31 we can visualise in figure 5-5 the difference between measured LHCP and RHCP signal power to noise ratio, after the removal of the instants where the receiver has lost tracking resulting in the negative C/No's. It can be seen that in some cases the C/No at the LHCP is higher than the C/No measured in the RHCP chain indicated by the positive values in the figure 5-5 which means that the signal that is coming to the antenna after the reflection is no more right hand polarised causing the C/No at the Left chain to be higher due to its co polar gain towards the Left polarised multipath signal. For clarity a statistical representation of the delta C/No is done in figure 5-6 using a histogram

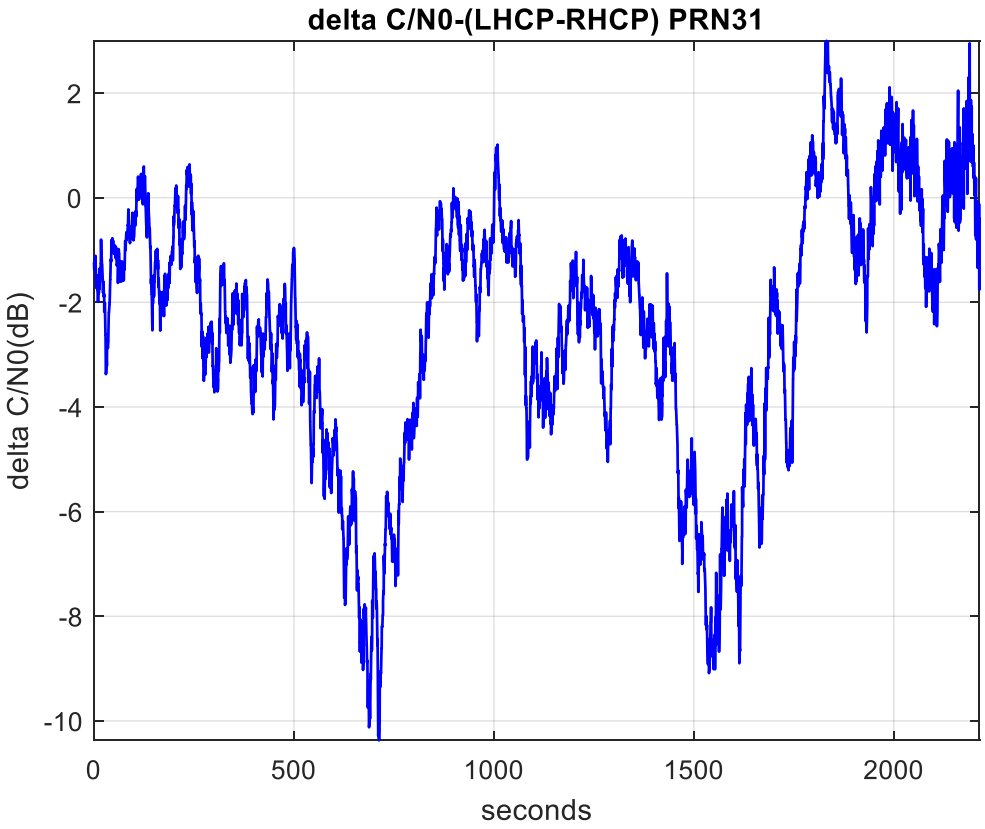

Figure 5-5 : The C/No difference at LHCP and RHCP

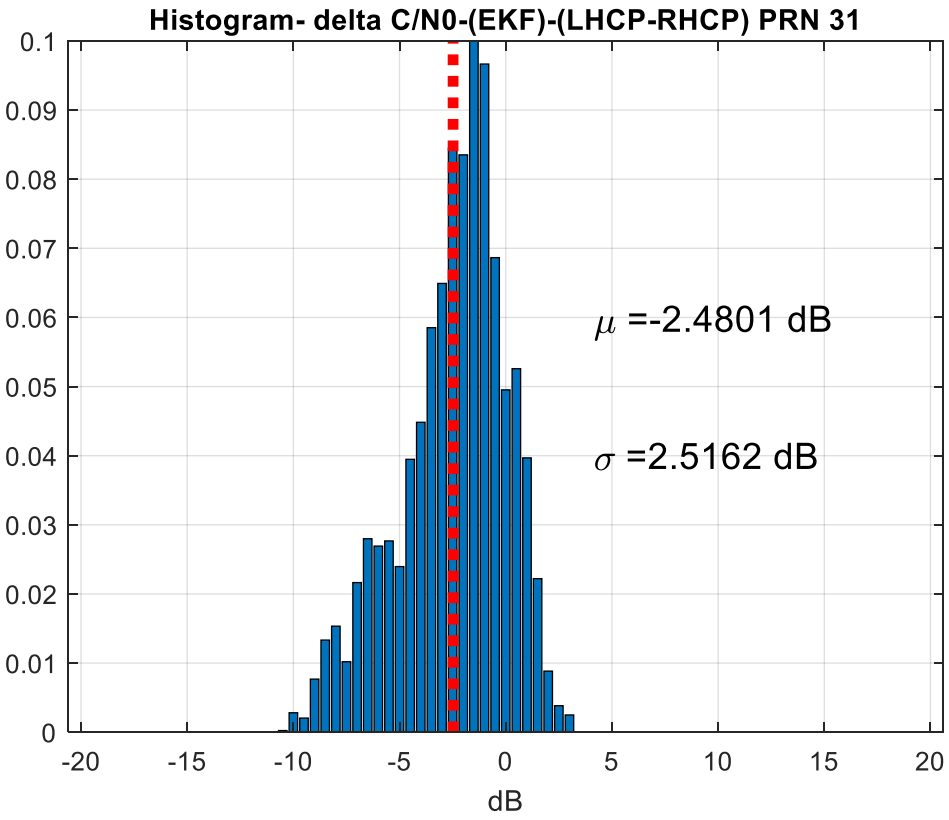

Figure 5-6 : Histogram for the difference in C/No

Apart from the I/Q observables and the information on the C/No's another measurement information logged into the dumplog files and used in the model is the difference in the pseudorange between the LHCP and RHCP antennas. This difference is represented by Є in the signal model of the LHCP chain and this also acts as the relationship between the RHCP and LHCP chain models. This difference in case of PRN-31 is illustrated in figure 5-7.

The difference in the measured pseudorange at LHCP and RHCP can be taken as another indicating factor of multipath presence. Like the difference in C/No we can see that towards the end of the database the bias is higher. The statistical representation on this difference has been done with a histogram in figure 5-8.

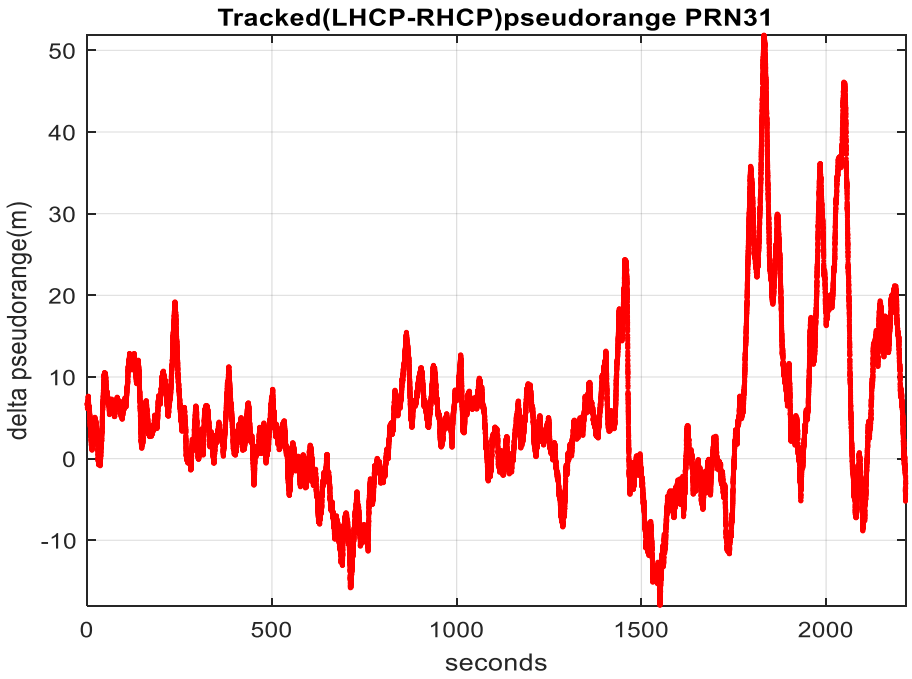

Figure 5-7 : The pseudorange difference between LHCP and RHCP

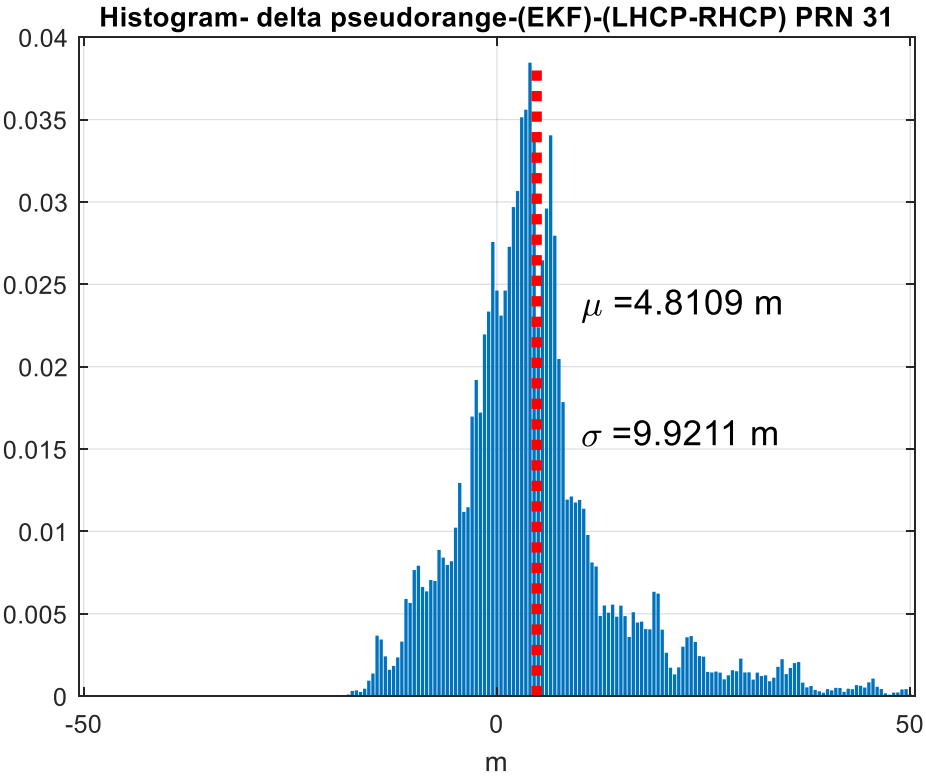

Figure 5-8 Histogram for the pseudorange bias

These differences in C/No and pseudorange along with being used in the algorithm itself can also be used to roughly characterize the multipath environment.

At a point in the algorithm the removal of data bit removal has been done from the observables. The bit removal is done by using the sign of I observables from the RHCP and multiplying this sign to the Q observables of RHCP and to both the I and Q observables of the LHCP.

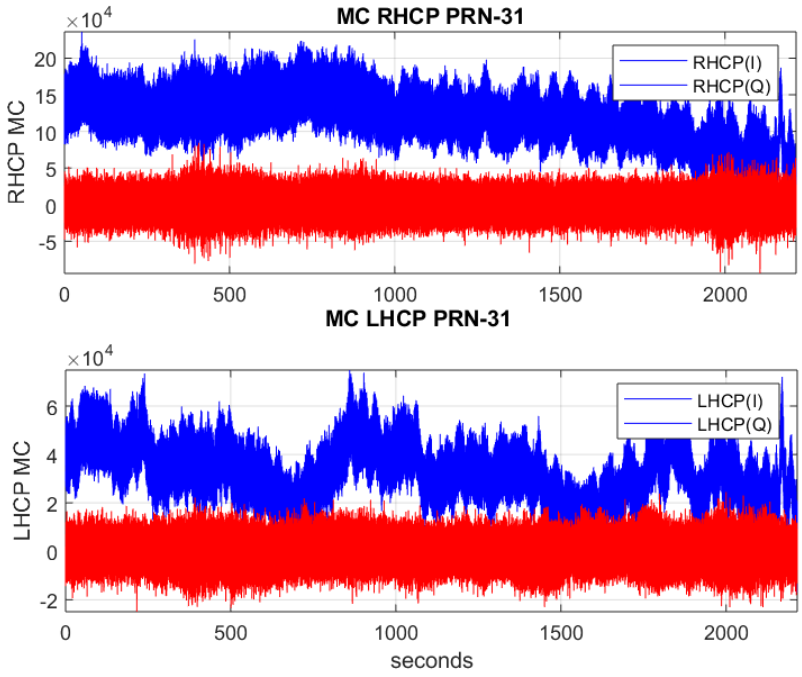

Figure 5-9 : RHCP and LHCP Multicorrelator Observables after bit removal

Bit removal has been considered in the work in order to simplify the EKF observables models. This process is considered to have negligible impacts at medium/high level RHCP signal, because in this case the bit removal process is considered error free. If instead the RHCP signal level is low, the process would be not acceptable, because of the error in the data bit estimation. The latter case is not considered here, because the LHCP tracking would likely be lost or multipath estimation very inaccurate because of insufficient LHCP power.

5.4 STATE MODELLING AND USE OF EKF TO MULTIPATH ESTIMATION PROBLEM

The signal received from the RHCP and LHCP chain consists of LoS as well as multipath components that are to be fed to the EKF in order to estimate the multipath parameters of our choice. We have seen the model of the received signals both RHCP and LHCP along with the parameters to be estimated in the previous section. However, the individual states that needs to be estimated needs to be modelled too in order to fit in the EKF algorithm we discussed in this chapter. We can see the signal model equations that we derived before as following:

- **RHCP Chain:**

$$(I_{\Delta m} + jQ_{\Delta m})_R = \alpha_{LoS}^{RR}.R(\delta\tau_{LoS}{}^{R} + \Delta m).e^{j(\delta\phi_{\mathrm{LoS}}^{RR})} + \alpha_{MP}{}^{R} \cdot R(\delta\tau_{LoS}{}^{R} - \delta\tau_{MP}{}^{R} + \Delta m).e^{j(\delta\phi_{\mathrm{MP}}^{R})}$$

- **LHCP Chain:**

$$(I_{\Delta m} + jQ_{\Delta m})_L = \alpha_{LoS}^{LR}.R(\epsilon + \delta\tau_{LoS}{}^{R} + \Delta m).e^{j(\delta\phi_{\mathrm{LoS}}^{LR})} + \alpha_{MP}{}^{L} \cdot R(\epsilon + \delta\tau_{LoS}{}^{R} - \delta\tau_{MP}{}^{R} + \Delta m).e^{j(\delta\phi_{\mathrm{MP}}^{L})}$$

The state vector to be estimated is given below:

$$X = [\alpha_{LoS}^{RR}\ \alpha_{MP}{}^{R}\ \delta\tau_{LoS}{}^{R}\ \delta\phi_{\mathrm{LoS}}^{RR}\ \delta\phi_{\mathrm{MP}}^{R}\ \delta\tau_{MP}{}^{R}\ \delta f\ \alpha_{LoS}^{LR}\alpha_{MP}{}^{L}\ \delta\phi_{\mathrm{LoS}}^{LR}\ \delta\phi_{\mathrm{MP}}^{L}\ \delta f_L]$$

In the above state vector, we can see that there are two more states δf and δf_L where δf is the frequency error to the RHCP and LHCP tracking chains and δf_L refers to the residual frequency error only in the LHCP chain. The vector of measurements from the 11 correlators for each chain is represented by Z.

$$Z = [I_{\Delta 1R}\ldots\ldots I_{\Delta 11R}\ Q_{\Delta 1R}\ldots\ldots Q_{\Delta 11R}\ldots\ldots I_{\Delta 1L}\ldots\ldots I_{\Delta 11L}\ Q_{\Delta 1L}\ldots\ldots Q_{\Delta 11L}]$$

Where the R in subscript stands for RHCP antenna and L stands for LHCP and $\Delta 1$ being the first correlator and $\Delta 11$ the last

Finally, we can see the models of individual states to be estimated as below:

1. α_{LoS}^{RR} (LoS signal amplitude at RHCP).

The LoS amplitude is modelled using the first order auto regressive process

$$\alpha_{LoS_{k+1}}^{RR} = \alpha_{LoS_k}^{RR} + w_{LoS}$$

2. α_{MP}^{R} (multipath amplitude at RHCP chain.)

This is modelled using the first order auto regressive process

$$\alpha_{MP_{k+1}}^{R} = A_{\alpha_{MP}}.\alpha_{MP_k}^{R} + w_{MP}$$

3. $\delta\tau_{LoS}^{R}$ (Code Phase offset between the LoS signal and locally generated signal.)

$$\delta\tau_{LoS_{k+1}}^{R} = \delta\tau_{LoS_k}^{R} + \delta T \cdot \delta f \cdot \frac{\lambda}{2\pi} + W_{\delta\tau_{LoS}^{R}}$$

4. $\delta\phi_{LoS}^{RR}$ (Average phase error for the RHCP LoS signal.)

It is linked to Doppler error as in the following expression

$$\delta\phi_{LoS_{k+1}}^{RR} = \delta\phi_{LoS_k}^{RR} + \frac{1}{2} \cdot \delta T \cdot \delta f + W_{\delta\phi_{LOS}^{RR}}$$

5. $\delta\phi_{\mathrm{MP}}^{R}$ (Average phase error for the RHCP multipath signal.)

As for the LoS, it is linked to the Doppler error, and in particular it is assumed to have the same Doppler of the LoS

$$\delta\phi_{MP_{k+1}}^{R} = \delta\phi_{MP_k}^{R} + \frac{1}{2} \cdot \delta T \cdot \delta f + W_{\delta\phi_{MP}^{R}}$$

6. $\delta\tau_{MP}{}^{R}$ (Code phase offset between the LoS signal and the multipath signal)

$$\delta\tau_{MP_{k+1}}^{R} = \delta\tau_{MP_{k+1}}^{R}.A_{\tau_{MP.}} + W_{\delta\tau_{MP}^{R}}$$

7. δf (frequency error between locally generated and the incoming signal)

$$\delta f_{k+1} = \delta f_{k+1} + \delta T \cdot \delta\alpha + w_{\delta f}$$

8. α_{LOS}^{LR} (Right Hand Polarised LoS signal amplitude at LHCP)

$$\alpha_{LoS_{k+1}}^{LR} = \alpha_{LoS_k}^{LR} + w_{LOS}$$

9. $\alpha_{MP}{}^{L}$ (multipath amplitude at LHCP).

$$\alpha_{MP_{k+1}}^{L} = A_{\alpha_{MP}}.\alpha_{MP_k}^{L} + w_{MP}$$

10. $\delta\phi_{LoS}^{LR}$ is the average phase error for the LoS signal at LHCP, for which an additional state of Doppler has been included in order to model the Doppler error in the LHCP tracking w.r.t. the RHCP one

$$\phi_{LoS_{k+1}}^{LR} = \delta\phi_{LoS_k}^{LR} + \frac{1}{2}\cdot \delta T \cdot (\delta f + \delta f_L) + W_{\delta\phi_{LoS}^{LR}}$$

11. $\delta\phi_{\mathrm{MP}}^{L}$ (Average phase error for the LHCP multipath signal, for which a

$$\delta\phi_{MP_{k+1}}^{L} = \delta\phi_{MP_k}^{L} + \frac{1}{2}\cdot \delta T \cdot (\delta f + \delta f_L) + W_{\delta\phi_{MP}^{L}}$$

12. δf_L (Residual frequency error at the LHCP side)

$$\delta f_{L_{k+1}} = \delta f_{L_k} + w_{\delta f_L}$$

Where the term denoted by w in all the equations with respective subscripts refer to the gaussian, uncorrelated , zero mean noise.

5.5 DETERMINATION OF STATE TRANSITION (F) MATRIX

The state equations modelled above are of the non-linear form:

$$x_k = f(x_{k-1}) + w_{k-1}$$

f is the system's dynamics of the nonlinear systems

To make the non-linear equations compatible for the Kalman filter we need to deduce them to the form

$$x_k = F.x_{k-1} + w_{k-1}$$

Where F is a transition matrix formed by taking the partial derivatives of the state equations with respect to each state. At each step this matrix F is applied to the state estimate in the previous iteration. The F in this case is a 12x12 matrix. In figure 5-9 it can be observed that the state transition matrix is a sparse matrix where most of the elements are zero.

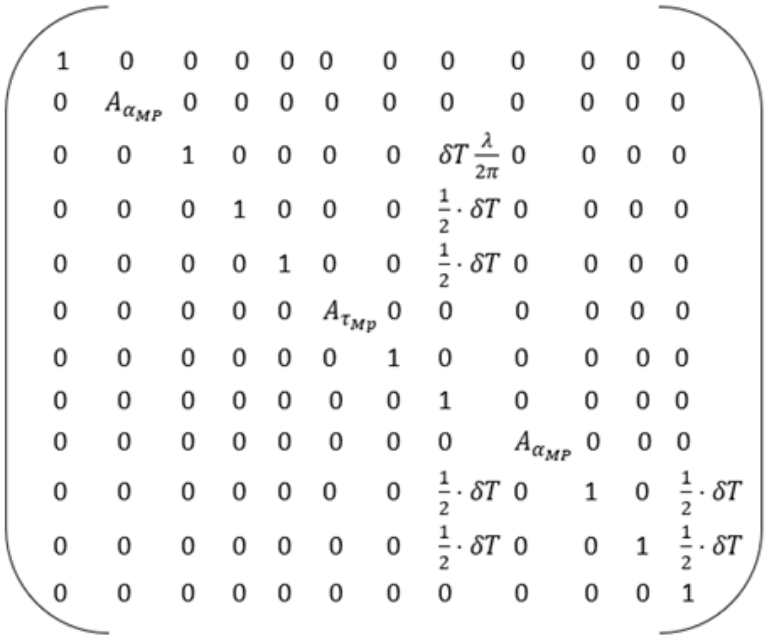

Figure 5-10 : State transition matrix (*F*)

5.6 DETERMINATION OF OBSERVATION (*H*) MATRIX

Similarly, the *H* matrix used in the prediction and correction steps of the EKF are calculated taking the partial derivative of the measurement equations (the overall signal models for RHCP and LHCP) with respect to the states to be estimated. The *H* matrix is the model of the observation that helps in mapping the observed and the true states.

$$z_k = h_k(x_k) + v_k$$

To make the non-linear equations compatible for the EKF they need to be deduced to the form

$$z_k = H_k . x_k + v_k$$

The *H* matrix is obtained by taking the Jacobian of the measurement model function and hence can be called as a Jacobian matrix. In other words, the partial derivative of the measurement model function with respect to each state to be estimated is taken. The H matrix can be derived as follows

$$\frac{\partial h}{\partial \alpha_{Los}^{RR}} = H(:,1) = [\ R(\delta\tau_{LoS}{}^{R} + \Delta m).e^{j(\delta\phi_{\mathrm{LoS}}^{RR})}\ ,\ zeros(1,11)]$$

$$\frac{\partial h}{\partial \alpha_{MP}^{R}} = H(:,2\ ) = [\ R(\delta\tau_{LoS}{}^{R} - \delta\tau_{MP}{}^{R} + \Delta m).e^{j(\delta\phi_{\mathrm{MP}}^{R})}\ ,\ zeros(1,11)\ ]$$

$$\frac{\partial h}{\partial \delta\tau_{LoS}^{R}} = H(:,3) = [\alpha_{LoS}^{RR}\ .\dot{R}\ (\delta\tau_{LoS}{}^{R} + \Delta m).e^{j(\delta\phi_{\mathrm{LoS}}^{RR})} + \alpha_{MP}{}^{R} \cdot \dot{R}\ (\delta\tau_{LoS}{}^{R} - \delta\tau_{MP}{}^{R} + \Delta m)\ .e^{j(\delta\phi_{\mathrm{MP}}^{R})}\ ,\ \alpha_{LOS}^{LR}\ .\dot{R}\ (\epsilon + \delta\tau_{LoS}{}^{R} + \Delta m).e^{j(\delta\phi_{\mathrm{LoS}}^{LR})} + \alpha_{MP}{}^{L} \cdot R\ (\epsilon + \delta\tau_{LoS}{}^{R} - \delta\tau_{MP}{}^{R} + \Delta m).e^{j(\delta\phi_{\mathrm{MP}}^{L})}\ ]$$

$$\frac{\partial h}{\partial \delta\phi_{LoS}^{RR}} = H(:,4) = [\alpha_{LoS}^{RR}.R(\delta\tau_{LoS}{}^{R} + \Delta m).\ j.\ e^{j(\delta\phi_{\mathrm{LoS}}^{RR})}\ ,\ zeros(1,11)\ ]$$

$$\frac{\partial h}{\partial \delta\phi_{MP}^{RR}} = H(:,5) = [\ \alpha_{MP}{}^{R} \cdot R(\delta\tau_{LoS}{}^{R} - \delta\tau_{MP}{}^{R} + \Delta m).j.e^{j(\delta\phi_{\mathrm{MP}}^{RL})}\ ,zeros(1,11)\ ]$$

$$\frac{\partial h}{\partial \delta\tau_{MP}^{R}} = H(:,6) = [\ -\alpha_{MP}{}^{R} \cdot \dot{R}\ (\delta\tau_{LoS}{}^{R} - \delta\tau_{MP}{}^{R} + \Delta m)\ .e^{j(\delta\phi_{\mathrm{MP}}^{R})}\ ,-\alpha_{MP}{}^{L} \cdot R\ (\epsilon + \delta\tau_{LoS}{}^{R} - \delta\tau_{MP}{}^{R} + \Delta m)\ .e^{j(\delta\phi_{\mathrm{MP}}^{L})}\ ]$$

$$\frac{\partial h}{\partial \delta f} = H(:,7) = [\ \alpha_{LoS}{}^{RR}.R(\delta\tau_{LoS}{}^{R} + \Delta m).\frac{1}{2} \cdot \delta T\ .j\ .e^{j(\delta\phi_{\mathrm{LoS}}^{RR})} + \alpha_{MP}{}^{R} \cdot R(\delta\tau_{LoS}{}^{R} - \delta\tau_{MP}{}^{R} + \Delta m).\frac{1}{2} \cdot \delta T\ .j\ .e^{j(\delta\phi_{\mathrm{MP}}^{R})}\ ,\alpha_{LoS}{}^{LR}.R(\epsilon + \delta\tau_{LoS}{}^{R} + \Delta m).\frac{1}{2} \cdot\ \delta T\ .j\ e^{j(\delta\phi_{\mathrm{LoS}}^{LR})} + \ \alpha_{MP}{}^{L} \cdot R(\epsilon + \delta\tau_{LoS}{}^{R} - \delta\tau_{MP}{}^{R} + \Delta m).\frac{1}{2}.\delta T\ .j\ e^{j(\delta\phi_{\mathrm{MP}}^{L})}]$$

$$\frac{\partial h}{\partial \alpha_{Los}^{LR}} = H(:,8) = [\ zeros(1,11),\quad R(\epsilon + \delta\tau_{LoS}{}^{R} + \Delta m).e^{j(\delta\phi_{\mathrm{LoS}}^{LR})}\ ]$$

$$\frac{\partial h}{\partial \alpha_{MP}^{L}} = H(:,9) = [\ zeros(1,11),\quad R(\epsilon + \delta\tau_{LoS}{}^{R} - \delta\tau_{MP}{}^{R} + \Delta m).e^{j(\delta\phi_{\mathrm{MP}}^{L})}\ ]$$

$$\frac{\partial h}{\partial \delta\phi_{LoS}^{LR}} = H(:,10) = [\ zeros(1,11),\quad \alpha_{LOS}^{LR}.R(\epsilon + \delta\tau_{LoS}{}^{R} + \Delta m).\ j.\ e^{j(\delta\phi_{\mathrm{LOS}}^{LR})}]$$

$$\frac{\partial h}{\partial \delta \phi_{MP}^{L}} = H(:,11) = [\,zeros(1,11), \quad \alpha_{MP}{}^{L}.R(\epsilon + \delta\tau_{LoS}{}^{R} - \delta\tau_{MP}{}^{R} + \Delta m).\ j.\ e^{j(\delta\phi_{\mathrm{MP}}^{L})}]$$

$$\frac{\partial h}{\partial \delta f_L} = H(:,12) = [zeros(1,11)\ , \alpha_{LoS}{}^{LR}.R(\epsilon + \delta\tau_{LoS}{}^{R} + \Delta m).\frac{1}{2}\cdot \delta T\ .j\ e^{j(\delta\phi_{\mathrm{LoS}}^{LR})} + \alpha_{MP}{}^{L}\cdot R(\epsilon + \delta\tau_{LoS}{}^{R} - \delta\tau_{MP}{}^{R} + \Delta m).\frac{1}{2}.\delta T\ .j\ e^{j(\delta\phi_{\mathrm{MP}}^{L})}]$$

In the above equations R refers to the ideal BPSK autocorrelation function calculated in MATLAB. $\dot{R}$ is the derivative of the BPSK auto-correlation. It is calculated using a sinc function because the ideal BPSK autocorrelation function is triangular and the derivative of a triangular function is a sinc function. The operations above produce a complex result and hence they must be separated into their real and imaginary parts to be fed into the Kalman filter. The above operation produces a 22x22 matrix and by separation we will finally have 44x44 matrix.

5.7 DETERMINATION OF STATE ERROR COVARIANCE (*P*) MATRIX

P matrix refers to the state error covariance matrix. The initial error covariance matrix is defined based on the state's initialisation error. If we are not very confident that the state values, we initialised are closer to the actual states then the initial covariance matrix P_0 must be very large. Instead if we are confident that our initial state vector is quite close to the actual state values, we can initialise P_0 to smaller values.

If *P* is initialised to 0 then the filter absolutely ignores the incoming measurements. However, if we initialise them to a very large value then the filter will trust only the measurements and the state models will be ignored.

So, it is important to take care that the choice of *P* must not be too less (i.e. 0) and not infinite too. Here P_0 has been chosen as a diagonal matrix with each diagonal element corresponding to the expected variance in the corresponding state.

The initial P matrix has been tuned by observing the effects of its change on the states estimation and finally the matrix resulting in the most stable estimation has been considered

5.8 DETERMINATION OF PROCESS COVARIANCE (Q) MATRIX

Q matrix refers to the uncertainty that can be expect in the modelled state equations. The performance of Kalman filter highly depends on how carefully and accurately the states are modelled.

Q matrix includes all the modelling errors and other uncertainties in the state equations themselves. It includes any driving inputs that could cause the state vector to deviate from the noise free state vector transition model.

In any case it is important to be very careful to never initialise the matrix Q to zeros because the filter will assume that the model is free of all errors. This will cause the filter to just rely on the model and completely ignore any measurement data that is fed to it.

In literature various ways have been mentioned to estimate the error covariance and noise covariance matrices . For example, in [13] an adaptive way to determine the matrix Q and R by the use of innovation has been described where the matrices get automatically updated depending on the measurements and predictions. Similarly, in [14] a study about various techniques like Expectation Maximization (EM), correlation techniques and covariance matching techniques for adaptive estimation of R and Q matrices have been discussed and a very new method called as Reference Recursive Recipe (RRR) has been introduced and analysed.

However, in our case resorting to those methods led to the Kalman gain matrix being very badly conditioned and almost singular so it was decided to have a fixed process noise covariance matrix (Q) initialised at the beginning of the process.

The Q matrix was initialized by observing the effects on states estimation and the most suitable Q matrix was finalised. The process noise covariance matrix (Q) remains constant throughout all Kalman iterations.

5.9 DETERMINATION OF MEASUREMENT NOISE COVARIANCE (R) MATRIX

The measurement noise can be modelled as a zero mean white noise process with Gaussian distribution. v(t)~N(0,R), where R represents the covariance matrix. The R matrix is produced by estimating the standard deviation of the measurements. Since we are working on the absolute values of I and Q samples the noise components remain no more gaussian but change into folded normal distribution. The relationship between the mean and variance of the gaussian distribution and folded normal distribution [15] can be shown as below:

$\sigma_y^2 = \mu^2 + \sigma^2 - \mu_y^2$ .....(1)

$\mu_y = \sigma \cdot \sqrt{\frac{2}{\pi}} \cdot e^{-\frac{u^2}{2\sigma^2}} + \mu \cdot erf\left(\frac{u}{\sqrt{2\sigma^2}}\right)$ .....(2)

Where: σ_y^2 and μ_y^2 are the variance and mean respectively of folded normal distribution.

: σ^2 and μ^2 are the variance and mean respectively of the original gaussian distribution.

From the calculated variances of the new folded normal distribution of the samples we have to estimate the variances of the old Gaussian distributed samples, and the assumptions and calculations made in doing so for the RHCP and LHCP side is shown below:

5.9.1 RHCP(Q) ,LHCP(Q):

In Q there is no signal, so we can assume that $\mu = 0$ So equation (1) can be written as

$\sigma_y^2 = \sigma^2 - \mu_y^2$....(3)

For the clarity of the above statement we can see the following figure. The red denotes the Q signal component which is around zero for both RHCP and LHCP.

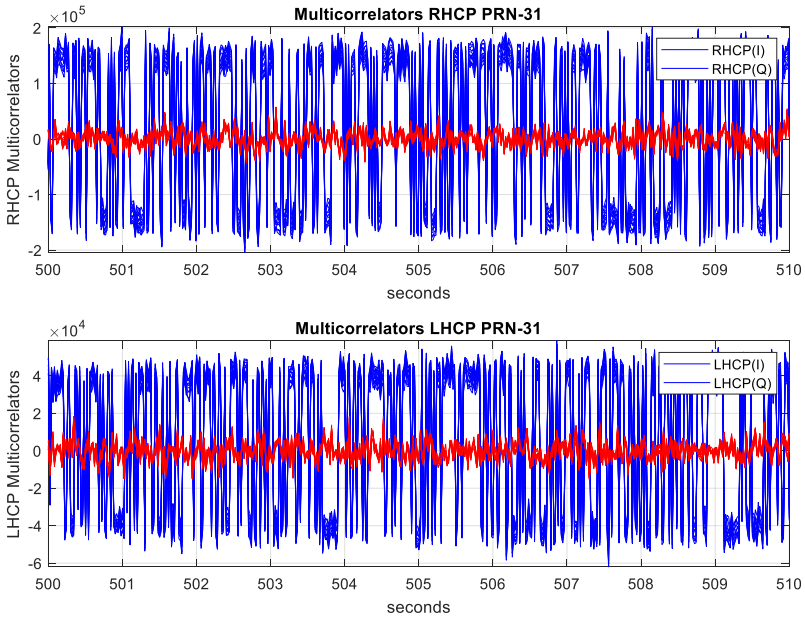

Figure 5-11 : Original RHCP and LHCP multi-correlators observables

Similarly, in equation 2 with the original mean equals to zero so the exponential term deduces to 1 and the erf term to zero

$$\mu_y = \sigma \cdot \sqrt{\frac{2}{\pi}} \quad \ldots\ldots(4)$$

Replacing (4) in (3), we get

$$\sigma^2 = \frac{\sigma y^2}{\left(1-\frac{2}{\pi}\right)} \ldots(5)$$

Equation (5) was used to calculate the noise of the Q- signal components.

5.9.2 RHCP(I),LHCP(I) :

In the I components the presence of signal is much higher than the noise as we can see in the above figure. i.e. $\mu^2 \gg \sigma^2$

In this case equation 1 deduces to $\sigma_y^2 = \sigma^2$ …(6)

Hence the noise in the I-components was estimated using equation 6. Following the above assumptions and deductions the estimated variance of the I and Q components is shown in the figure below.

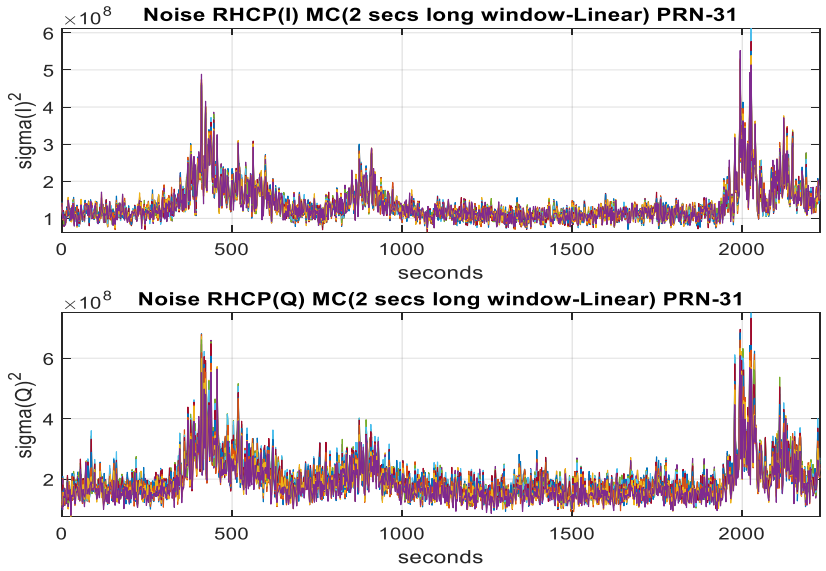

Figure 5-12 : variance in I and Q multicorrelators samples for RHCP

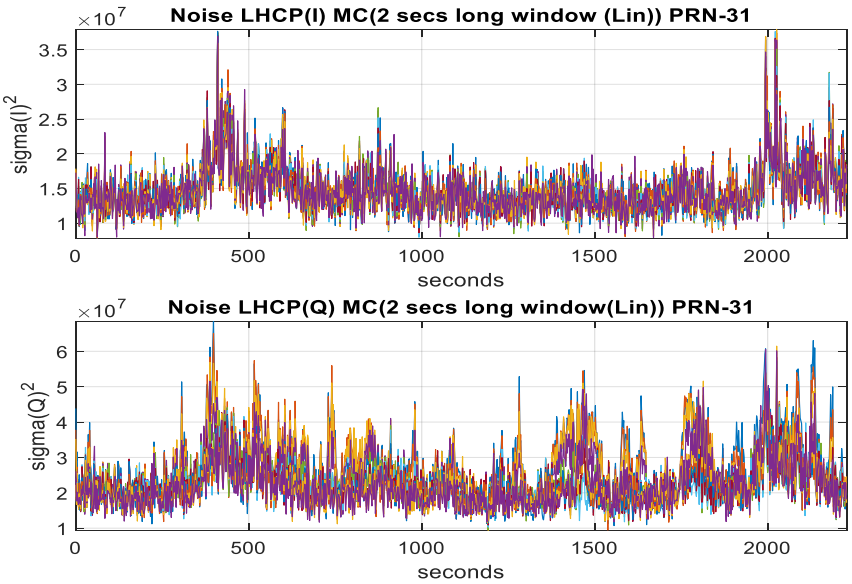

Figure 5-13 : variance in I and Q multicorrelator samples for LHCP

The I and Q observables are fed into the Extended Kalman Filter as separate entities rather than a complex quantity. Coherently , the noise terms used into the calculation of the *R* matrix is calculated separately for I and Q samples. From the figures above we can see that the noise components in 11 multicorrelators is the same. Considering that the multipath occurs with a positive delay, the first multicorrelator can be assumed to be least affected by the multipath and the noise estimated as the pure noise. Hence, the first multicorrelators variance can be chosen as the noise to be fed into the Kalman Filter.

Furthermore, the designing of the *R* matrix is done in the following way:

1. The variance of the first Multicorrelator observables fill up the diagonal of the R matrix.
2. Considering the noise is correlated among the Multicorrelators. The noise for the rest of the Multicorrelators is computed by correlating the noise in the first correlator as a function of the distance of the first correlator to the respective correlators. An ideal BPSK autocorrelation function is used for this purpose.

5.10 CONSTRAINED EKF

In the estimation tool along with the conventional EKF there is the possibility to switch to Constrained EKF that is expected to help the Kalman filter to converge. The constrained EKF is a modified version of EKF, in which after step 1 and 2 of EKF (see *§5.2*), a new contribution is included at the correction step, using the available constrains: The step of correction which is different compared to the conventional EKF can be seen as below.

- **Step 3 -Correction for Constrained EKF**

The Kalman gain at time instant k is calculated using the covariance matrix from the step 2($P_{k|k-1}$), the linearized observation matrix (H_k), and the measurement noise covariance matrix(R_k)

$$K_k = P_{k|k-1} \cdot H_k^T \left(H_k \cdot P_{k|k-1} \cdot H_k^T + R_k\right)^{-1}$$

The posteriori covariance matrix at time instant k can be calculated as given below:

$$P_k = (I - k_k H_k) P_{k|k-1}$$

The posteriori state estimate in case of Extended Kalman Filter (EKF) is given by the following expression

$$\hat{x}_{k|k} = \hat{x}_{k|k-1} + K_k\left(Z_k - \hat{Z}_k\right)$$

Consequently, using the posterior estimate calculated in the correction step of the EKF, the posteriori state estimate at instant k can be calculated as given below which is different than in case of conventional EKF.

$$\hat{x}_{k|k} = \hat{x}_{k|k-1} - P_k . D' . inv(D . P_k . D') . (D . \hat{x}_{k|k-1} - c)$$

Where,

D is obtained from the linearization of the constraining equations and

$$c = b - g(x) + D . \hat{x}_{k|k-1}$$

Where,

$$b = \begin{bmatrix} b_1 \\ b_2 \end{bmatrix}$$

$g(x)$ is the constraining function for the Kalman filter.

In our algorithm we have applied a constraint each on RHCP and LHCP. The constraint is that the absolute values of the early minus absolute values of the late is equal to zero on average. It can be shown as:

For RHCP,

$$g_{r(x)} = \ b_1$$

$$g_{r(x)} = \sqrt{I_E^2 + Q_E^2} - \sqrt{I_L^2 + Q_L^2} = 0$$

After some simplification the equation becomes:

$$g_{r(x)} = \{\alpha_{LOS}^{RR^2} \cdot R^2\big(\delta\tau_R + \Delta m(e)\big) + \alpha_{MP}^{R^2} \cdot R^2(\delta\tau_{LOS}{}^R + \Delta m(e) - \delta\tau_{MP}{}^R) + 2 \cdot \alpha_{\text{Los}}^{RR} \cdot$$

$$\alpha_{MP.}^{R} R\big(\delta\tau_R + \Delta m(e)\big) \cdot R(\delta\tau_{LOS}{}^R + \Delta m(e) - \delta\tau_{MP}{}^R) \cdot \cos(\delta\phi_{LOS}^{RR} - \delta\phi_{MP}^{R})\}^{1/2} \ - \ \{\alpha_{LOS}^{RR^2} \cdot$$

$$R^2\big(\delta\tau_R + \Delta m(l)\big) + \ \alpha_{MP}^{R^2} \cdot \ R^2(\delta\tau_{LOS}{}^R + \Delta m(l) - \delta\tau_{MP}{}^R) + 2 \cdot \alpha_{\text{Los}}^{RR} \cdot \alpha_{MP.}^{R} R\big(\delta\tau_R +$$

$$\Delta m(l)\big) \cdot \ R(\delta\tau_{LOS}{}^R + \Delta m(l) - \ \delta\tau_{MP}{}^R) \cdot \cos(\delta\phi_{LOS}^{RR} - \delta\phi_{MP}^{R})\}^{1/2} \ = \ 0$$

In the above equation $b_1 = 0$

Similarly,

for LHCP

$$g_{l(x)} = \ b_2$$

$$g_{l(x)} = \sqrt{I_E^2 + Q_E^2} - \sqrt{I_L^2 + Q_L^2} = 0$$

$$g_{l(x)} = \ \{ \ \alpha_{LOS}^{LR^2} \cdot R^2\big(\epsilon + \delta\tau_R + \Delta m(e)\big) + \alpha_{MP}^{L^2} \cdot R^2(\epsilon + \delta\tau_{LOS}{}^R + \Delta m(e) - \ \delta\tau_{MP}{}^R) + 2 \cdot \alpha_{\text{Los}}^{LR} \cdot$$

$$\alpha_{MP.}^{L} R\big(\epsilon + \delta\tau_R + \Delta m(e)\big) \cdot R(\epsilon \ + \delta\tau_{LOS}{}^R + \ \Delta m(e) - \delta\tau_{MP}{}^R) \cdot \cos(\delta\phi_{LOS}^{LR} -$$

$$\delta\phi_{MP}^{L})\}^{1/2} \ - \qquad \{\alpha_{LOS}^{RR^2} \cdot R^2\big(\epsilon + \delta\tau_R + \ \Delta m(l)\big) + \alpha_{MP}^{L^2} \cdot R^2(\epsilon \ + \delta\tau_{LOS}{}^R + \Delta m(l) -$$

$$\delta\tau_{MP}{}^R) + 2 \cdot \alpha_{\text{Los}}^{LR} \cdot \ \alpha_{MP.}^{L} R\big(\epsilon \ + \delta\tau_R + \Delta m(l)\big) \cdot R(\epsilon \ + \delta\tau_{LOS}{}^R + \Delta m(l) - \delta\tau_{MP}{}^R) \cdot$$

$$\cos(\delta\phi_{LOS}^{LR} - \ \delta\phi_{MP}^{L})\}^{1/2} \ = \ 0$$

In the above equation $b_2 = 0$

Where $\Delta m(e) = early\ correlator$

$\Delta m(l) = late\ correlator$

Then c in our case will be

$$c = zeros(2,1) - g(x) + D.\hat{x}_{k|k-1}$$

The *D* matrix is obtained by linearizing the constraint equations for both left and right side with respect to each state to be estimated. Finally, after replacing all the values we obtain the new state estimate given by:

$$\hat{x}_{k|k} = \hat{x}_{k|k} - P_k.D'.inv(D.P_k.D').(D.\hat{x}_{k|k-1} - c)$$

6 SET-UP DESCRIPTION

This chapter describes all the contributing factors used in the development of the work done in the thesis from the phase of reception of the signals to the final estimation of the multipath parameters. The setup described here consists of both the hardware (Dual Polarised Antenna, the receiver) and the software (the DPA toolbox) entities which finally facilitate the estimation of the multipath parameters. The overall framework can be seen in the following figure.

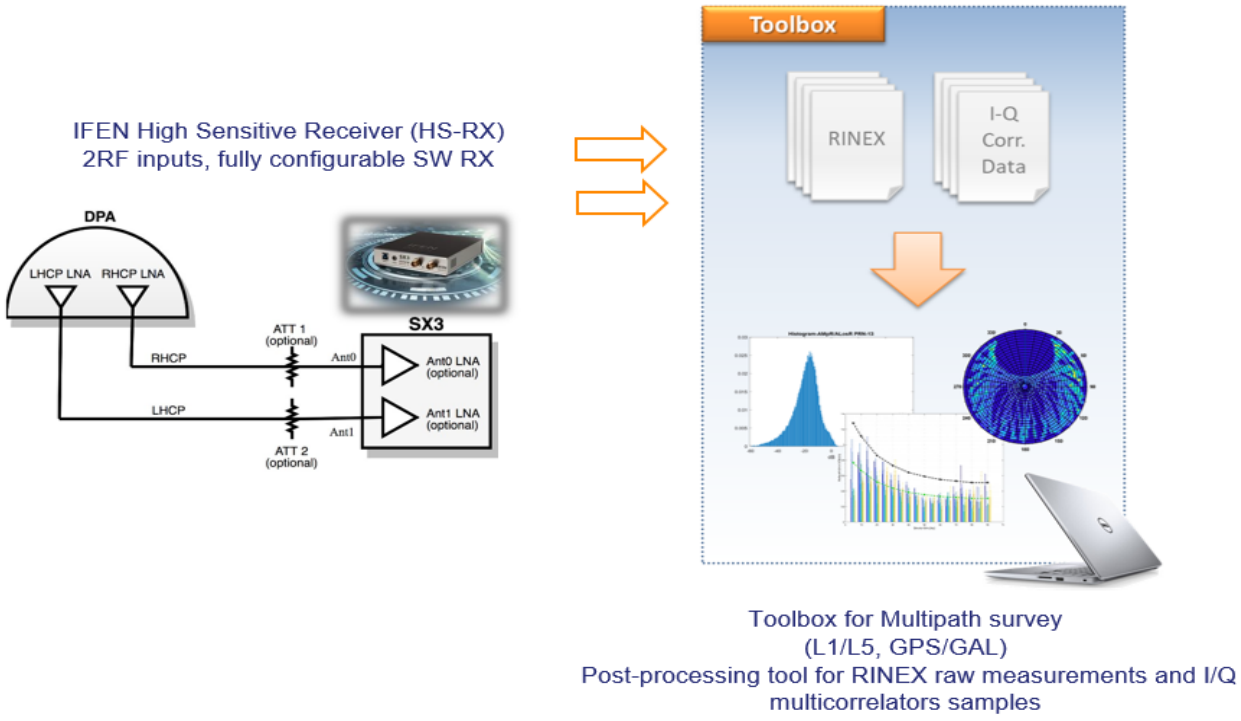

Figure 6-1 : A general setup description with antenna, receiver and toolbox

6.1 ANTENNA DESCRIPTION

Ideally, the GNSS signals coming from the satellites are RHCP but when they get reflected the signal turns partly into Left Hand Circularly Polarised(LHCP). Hence the received signal is a combination of both RHCP and LHCP signals. A conventional receiver that consists of only RHCP

antenna is highly sensitive to the RHCP signal and has an inbuilt anti-multipath feature attenuates the LHCP signal. On the contrary, a Dual Polarised Antenna is also able to respond to LHCP component of the Multipath signals simultaneously. If the signal is highly affected by multipath then it can be said that the output on the LHCP antenna chain is higher than in the RHCP. This provides a way to characterise and estimate a multipath environment better and aids in its mitigation. In literature different Corner-Truncated Square patch antennas DPAs have been adopted for multipath NLOS detection and mitigation. A new DPA prototype has been developed in 2017 by Ingegneria dei Sistemi(IDS) for ground reference stations and it has been used in the frame of this study which can be seen in figure 6-2**.** The structure shown in this figure enclosed RHCP and LHCP sensitive antennas in a single frame with two different outputs.

Figure 6-2 : IDS DPA Back with dual-output RHCP/LHCP and Side (RADOME)

The L1 radiation patterns for RHCP and LHCP antennas can be seen as below. Blue curves represent the co-polar gain and the red curves denote the cross-polar gain.

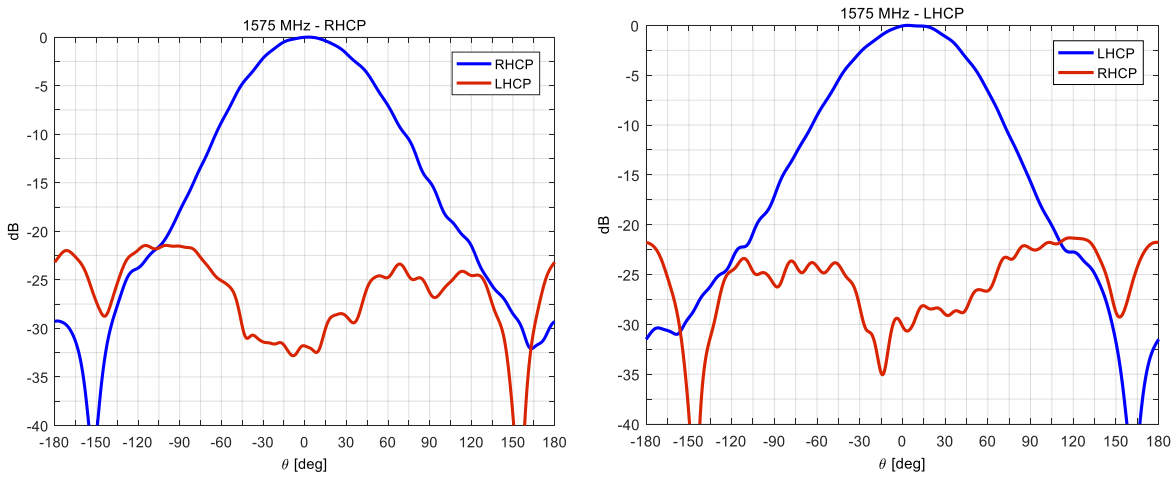

Figure 6-3 : IDS DPA L1 band co-polar (blue), cross-polar gain patterns (red)

6.2 RECEIVER

The signals from the satellites were received by the High sensitivity IFEN SX3 navigation receiver, adopted in the frame of the project because of its capability of receiving two polarisations per RF band. The receiver works with one or two inputs, with Dual polar RF inputs and has a Multi-frequency RF frontend. Figure 6-4 shows the configuration of the receiver with dual RF version that has been used in the frame of this thesis.

Figure 6-4 : Front panel of the SX3 frontend housing (dual RF version)

The SX3 frontend is a fully programmable GNSS receiver frontend able to cover all current GNSS signals within L-band and the IRNSS signals within the S-Band. One single SX3 front end unit may support four out of five RF-bands. The receiver has real time and post processing

operating mode. The post processing mode enables a broad variety of possibilities for algorithm development and signal analysis. The receiver can provide us with several output and log files.
The SX3 not only offers output within the graphical user interface but also output files are generated and live output data is provided depending on the chosen configuration. In our case we use the Multicorrelators dumplog files generated using the dual RF mode. The receiver generates an output .dumplog file that consists of the status of the tracking channel of a satellite signal after each primary integrate and dump period. The primary integrate and dump period equals to the primary PRN code length .

This dumplog file consists of many signal information like GPS receiver time, week, Code Pseudorange, Phase Pseudorange, the states of the tracking loops, the estimated signal power(C/No), code phase error, carrier phase error, frequency tracking error, and the In-phase and Quad-phase output of 11 multicorrelators for both the RHCP and the LHCP chain of the receiver.
The receiver is fed by the “Dual Polarised antenna” and it tracks the same satellites on the RHCP and LHCP antenna’s outputs.

The receiver for each channel in tracking provides n=11 equally spaced (configurable) multicorrelators, whose output along with an appropriate signal model is used for the multipath parameters’ estimation. The algorithm developed for multipath estimation will be finally integrated in a post-processing toolbox that acts in an open loop mode and does not provide any feedback to the High Sensitivity Receiver Processing. The algorithm will be constrained to process only the HS-RX (i.e. multi-correlators) from RHCP/LHCP antennas and not providing any feed back to the HS-RX processing for multipath estimation, i.e. open loop w.r.t. the tracking process.

6.3 DPA TOOLBOX

As stated earlier the overall toolbox has different functionalities in terms of Multipath surveying and analysis and the work presented here is a portion of the whole toolbox. The toolbox can be used to survey the prospective sites for the GNSS ground reference stations for the presence of multipath and RF interference. The results of the analysis done using the toolbox can be used to accept, characterize and inspect the onsite installed antenna and receiver platforms. The toolbox works on multi- frequency and multi-constellation GNSS measurements.

The toolbox can perform analysis of the raw measurements either from one single antenna or dual antenna. In single antenna analysis the figures of merit are used to characterize the single antenna performance and do a conventional site survey assessment. Whereas in the dual antenna combination analysis the Figures of merit are generated by specific processing on raw measurements from two different antenna + receiver streams (i.e. figures for multipath correlation between two antennas which are not located in the same position, combination of RHCP/LHCP antennas).

The single frequency analysis done using the toolbox is used to introduce the tracking performance. The dual frequency analysis produces the figures of merit which need the contribution of two frequencies measurements. These metrics are typically used for Multipath survey characterization (iono free results). It does a characterization and statistical analysis of the site using the raw measurements from the RINEX files. Apart from this various pre-correlation and post-correlation techniques are used to do in-depth analysis of RF interference and multipath using the IF samples and I/Q multicorrelator outputs [1].

The toolbox can also perform multipath parameters estimation using an EKF. The Multipath estimation is done on the I/Q multicorrelator dumplogs. This part of the toolbox is the focus of the thesis work. The multipath parameters estimation is done using the data from the dual antenna

(RHCP and LHCP) for a single frequency. The flow of the toolbox in a sequential order focusing only on the part of EKF as it is the scope of the thesis is with the help of following figures.

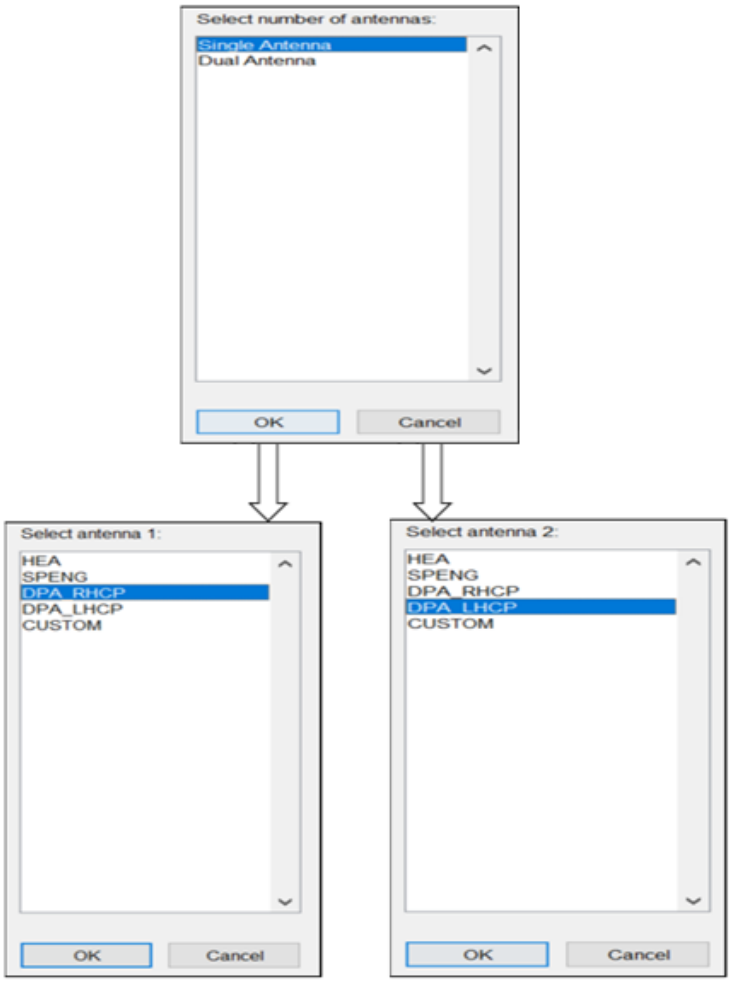

Figure 6-5 : Antenna selection phase of the toolbox

In the figure above we can see that the user operating the toolbox is first asked to select the number of antennas. As EKF-MP analysis is done using data from both the RHCP and LHCP antennas , dual antenna is selected. In the next step the user selects the data from DPA RHCP antenna and DPA LHCP antenna as the first and the second antenna respectively.

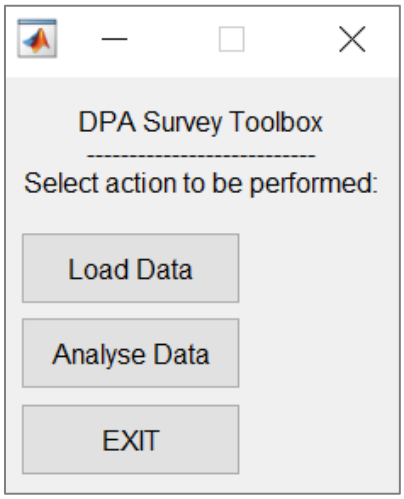

Figure 6-6 : Basic flow of the toolbox leading to EKF-MP Analysis

After the step presented by figure 6-5, the user can select the option to load the data , analyse the data or end the application execution as seen in figure 6-6. After the user selects the analyse option another dialog box asking for the kind of analysis to be done appears and the option Multicorr EKF-MP Analysis is to be chosen as seen in figure 6-7.

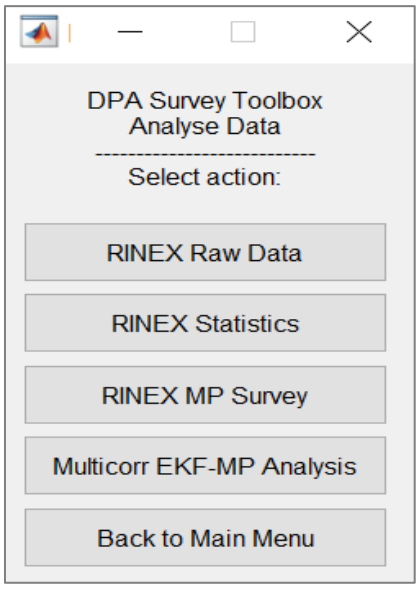

Figure 6-7 : Selection of the type of analysis to be performed

After the selection of the Multi-correlator based EKF-MP analysis the user shall see the pop-up window as shown in figure 6-8. This is used to make the selection of the RHCP dumplog data of

the PRN the user wants to process. When the user selects the RHCP dumplog of a certain PRN a corresponding LHCP dumplog for the same PRN gets automatically selected.

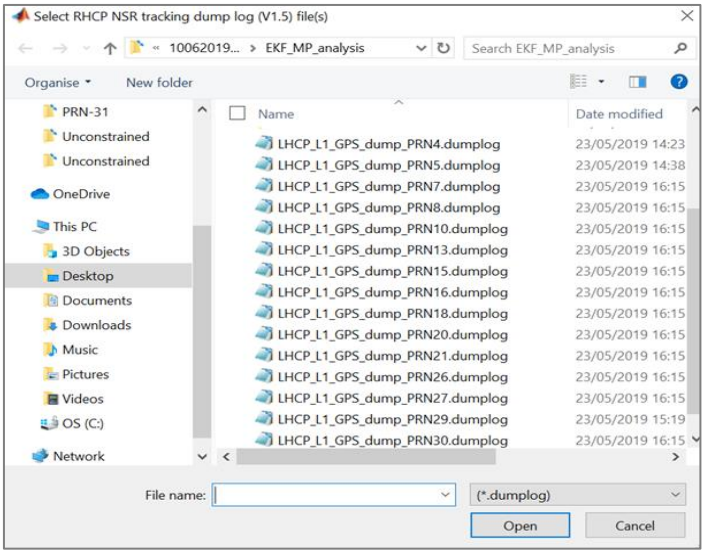

Figure 6-8 : Selection of the PRN dumplog for EKF analysis

The pop-up window in figure 6-9 allows the user to select the number of samples to average in each multicorrelator to be fed into the Kalman filter. If no averaging is to be applied, 1 is written in the dialog box. This is useful when we want to use the constrained EKF.

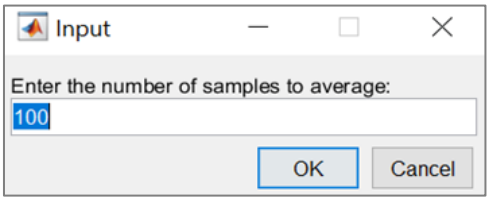

Figure 6-9 : Selection of number of samples to average

The pop-up window in figure 6-10 allows the user to select the initial sample number to start the Multipath analysis, the length of the window used in calculation of the noise Standard Deviation (STD) to be fed to EKF algorithm, the last sample of the analysis interval, the early correlator index among dumplog entries, the late correlator index among dumplog entries and finally the prompt correlator index among dumplog entries.

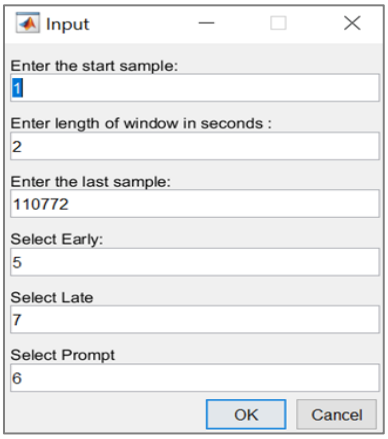

Figure 6-10 : Selection of necessary parameters for EKF estimation

The final pop-up window shown in figure 6-11 allows the user to select whether to perform multipath estimation using EKF or Constrained EKF (C-EKF). If the user enters 0 in the dialog box, the toolbox performs EKF analysis whereas if he selects 1 it activates constrained EKF.

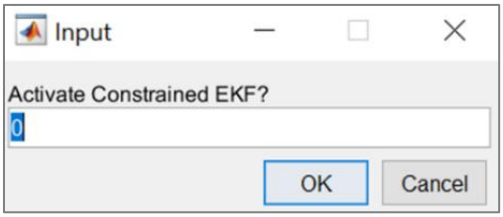

Figure 6-11 : Selection between EKF or Constrained EKF

7 LIVE TESTS AND RESULTS

The focus of this chapter is to visualise the multipath parameters by applying the signal model and techniques discussed in chapter four and five respectively. The analysis is done on the real data that was acquired in the rooftop of ESTEC (European Space Research and Technology Centre), Noordwijk, Netherlands.

7.1 ANALYSIS

The functionalities of the overall toolbox were discussed in DPA toolbox section of the previous chapter (*§6.3*). In this chapter only the EKF multipath parameters estimation feature of the toolbox which is the argument of the thesis is focused and the results presented.

In the work developed in the thesis, outputs logged into respective dumplog files for both RHCP and LHCP chains containing I/Q multicorrelators observables, pseudorange, C/No values , carrier phase etc have been exploited for multipath estimation. In this section the analysis done by processing PRN 31 with EKF scheme is reported. Before moving to the EKF analysis, a very high-level analysis of the results obtained by processing the RINEX raw data using the multipath survey feature of the toolbox is reported . In particular, the time correlated error is studied focusing on the low elevation angles which is more likely to be affected by multipath. The analysis is done with the I/Q data of PRN-31 can be seen in figure 7-1.

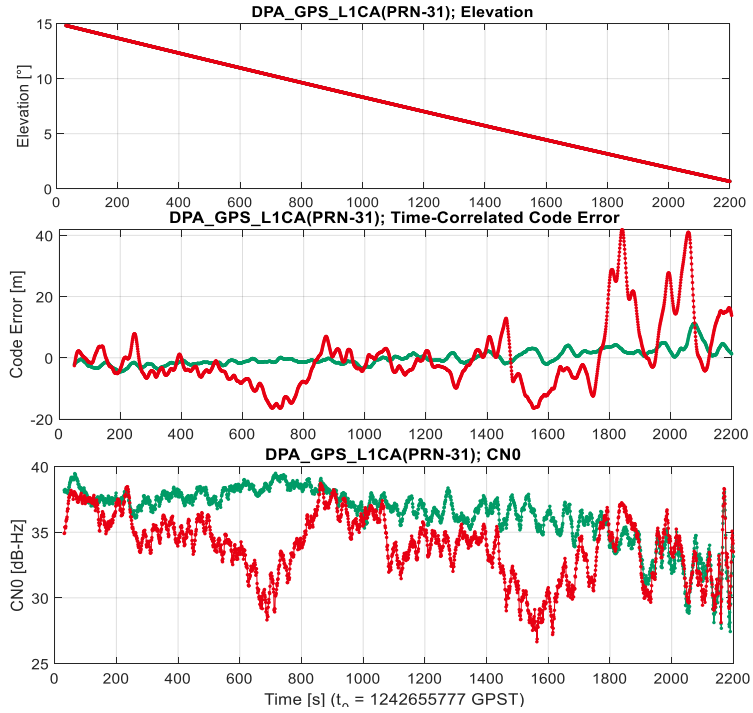

Figure 7-1 : Elevation, Code error and CN0 for RHCP and LHCP(PRN-31)

In the first subplot of the above figure we can see the elevation angle of PRN-31 which is in between 0-15°. The main interest lies in the lower elevation angle portion as the PRN's are most affected by the multipath in lower elevation. The second subplot of the above figure illustrates the time correlated error on RHCP denoted by green which is almost constant in the beginning.

However, the trend of the code error on RHCP changes around the 2000th seconds which is a very low elevation angle region as well suggesting the possible presence of multipath. In the third subplot of the above figure, drawn in green, we can see the behaviour of measured C/No for RHCP. In the case of the C/No too we can see the irregularities with respect to the usual behaviour around the 2000th second i.e. the low elevation region. In those regions. We can see that the C/No at the LHCP is higher than the C/No measured in the LHCP chain which means that the signal that is coming to the antenna after the reflection is no more right hand polarised causing the C/No at the Left chain to be higher due to its co polar gain toward the Left polarised multipath signal.

The code error for the LHCP denoted by red in the second subplot instead is quite evident from the beginning and is especially higher in the low elevation region. We can better visualise the RHCP and LHCP code errors in the following figures

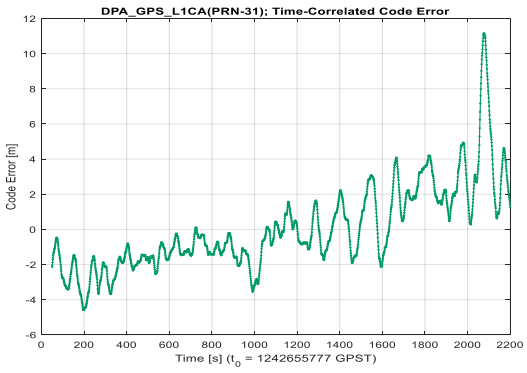

Figure 7-2 : Code error at the RHCP

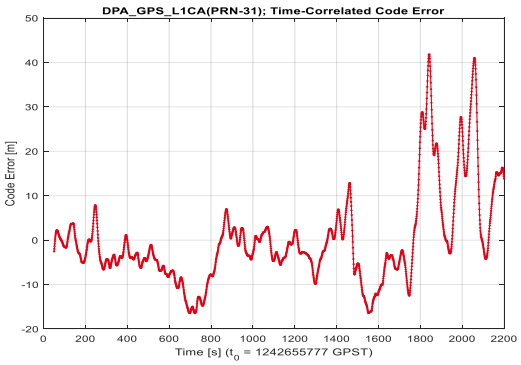

Figure 7-3 : Code error at LHCP

The multicorrelators observables to be fed to the Kalman filter after the processing of data and filtering the unnecessary outliers, negative C/No's and bit removal can be seen in the figures below:

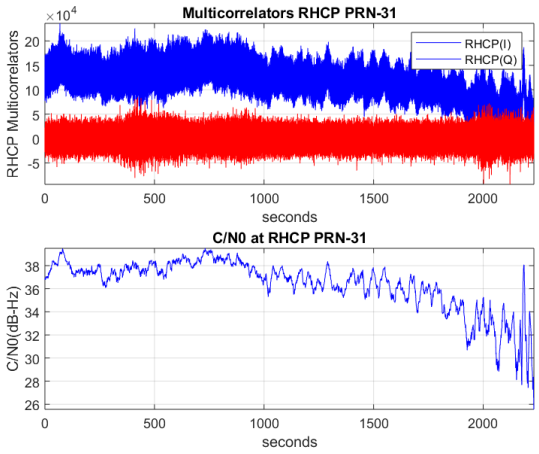

Figure 7-4 : RHCP MC's with C/No

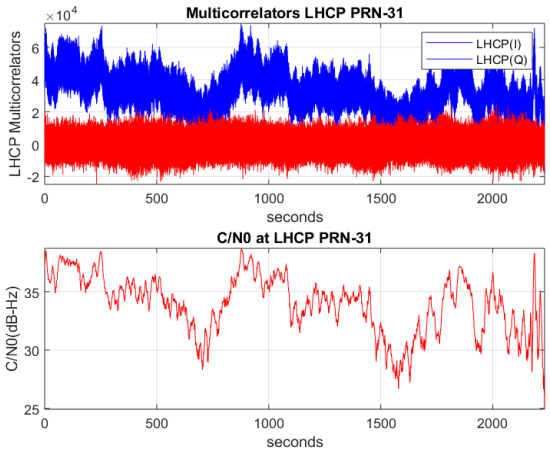

Figure 7-5 : LHCP MC's with C/No

It was discussed in chapter five that the measurement noise matrix denoted by *R* is estimated using the variance of the first multicorrelators for both RHCP and LHCP. The noise to be fed to the EKF for PRN-31 can be visualised in the pictures below.

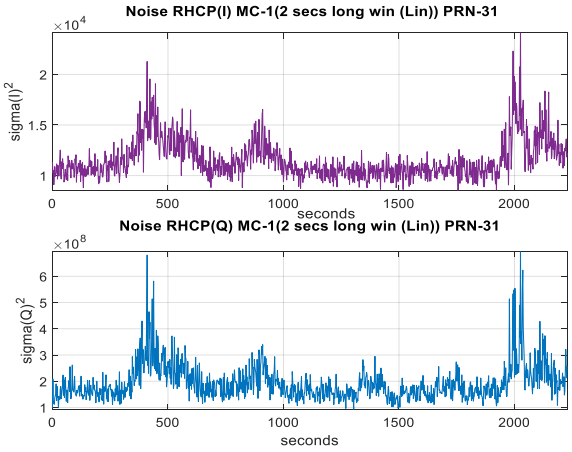

Figure 7-6 : RHCP Noise

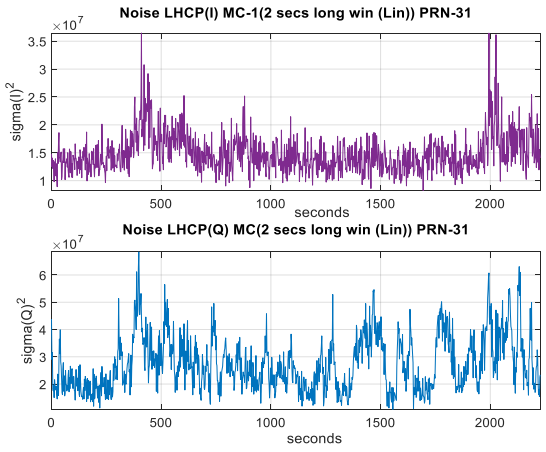

Figure 7-7 : LHCP Noise

In above figures we can see that in case of RHCP the noise in I and Q samples are similar whereas in case of LHCP the noise in I and Q samples are not so similar. This is an indication of a possible multipath presence. The whole set of multicorrelator values (i.e. 11) are also generated and reported below focusing on specific observation times.

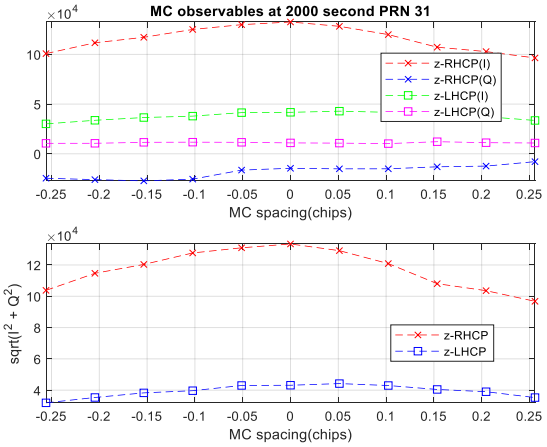

Figure 7-8 : MC observables at 2000th second

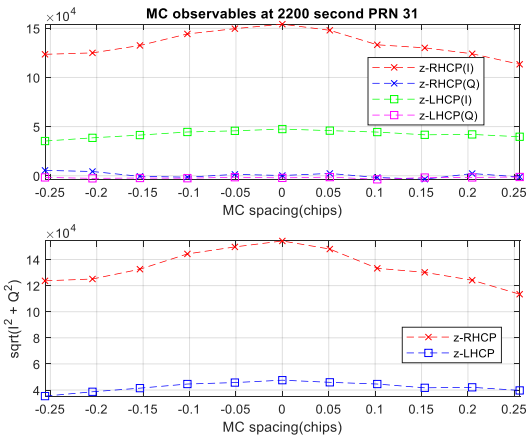

Figure 7-9 : MC observables at 2200th second

On the first subplot of both the figures 7-8 and 7-9, the I/Q correlators is shown for RHCP and LHCP chains with respect to its own tracking prompt value (different tracking for RHCP and LHCP chains). On the bottom chart, the root of the sum of the square of I and Q is also shown. In the figures above the presence of Multipath can be suggested by:

- The non-symmetric share of the sampled correlation functions(In-phase values)
- Residual power on Q-phase samples
- LHCP power higher than the one expected by the LoS received in cross-polar mode

7.1.1 EKF Estimations

It was discussed in chapter 5 that EKF works on the principle of prediction and correction of the prediction made. The correction to the predicted estimate is done using a factor called innovation. Innovation refers to the difference between the actual measured multicorrelators observables and the predicted measurements using the measurement models for both RHCP and LHCP chains.

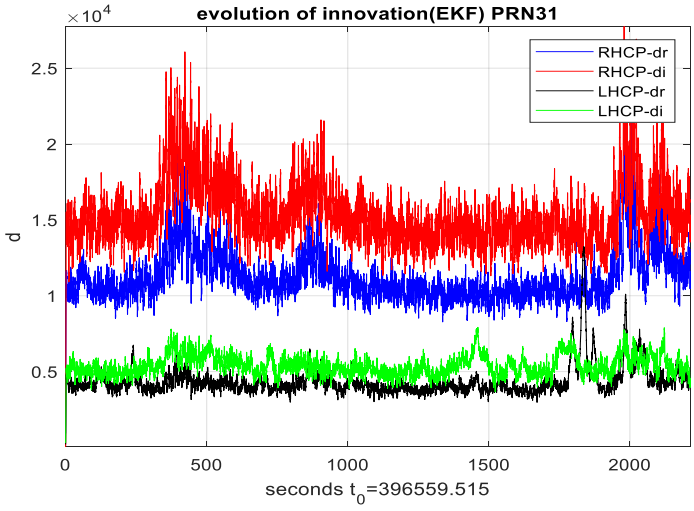

Figure 7-10 : Evolution of Innovation

The more stable and lower the innovation is, the better is the Kalman Filter estimation. After setting up all the noise matrices as discussed in the chapter 5 (see §5.7, §5.8, §5.9) and after many trials we reached to a stable point where we obtained the innovation as shown in figure 7-10.

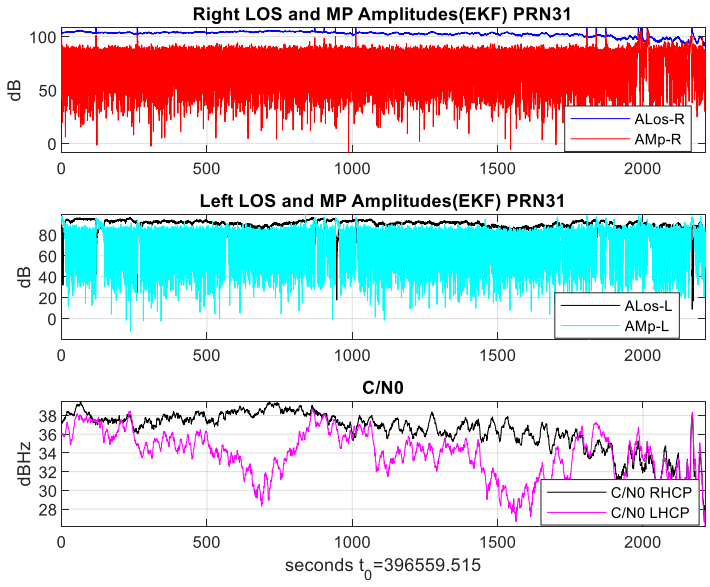

Figure 7-11 : LoS and multipath amplitude estimation in dB

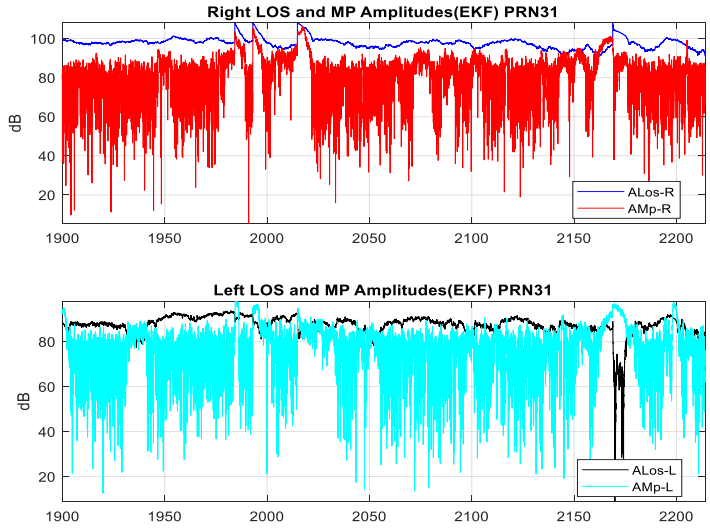

Figure 7-12: Zoomed in view of the LoS and multipath amplitude in last seconds

The figures in 7-11 and 7-12 above illustrate the LoS and Multipath estimated by the EKF, where the latter contains the zoom on a specific time interval where multipath presence is expected. The estimation in above figure shows that the multipath component in both the RHCP and LHCP is non-existent or very low. However, towards the end we can see some peaks suggesting the possible presence of multipath. The presence of the multipath in this area was also backed up by the analysis that was done for figure 7-1. The estimated LoS delay and the Multipath delay along with the generated histograms for statistical analysis can be seen below.

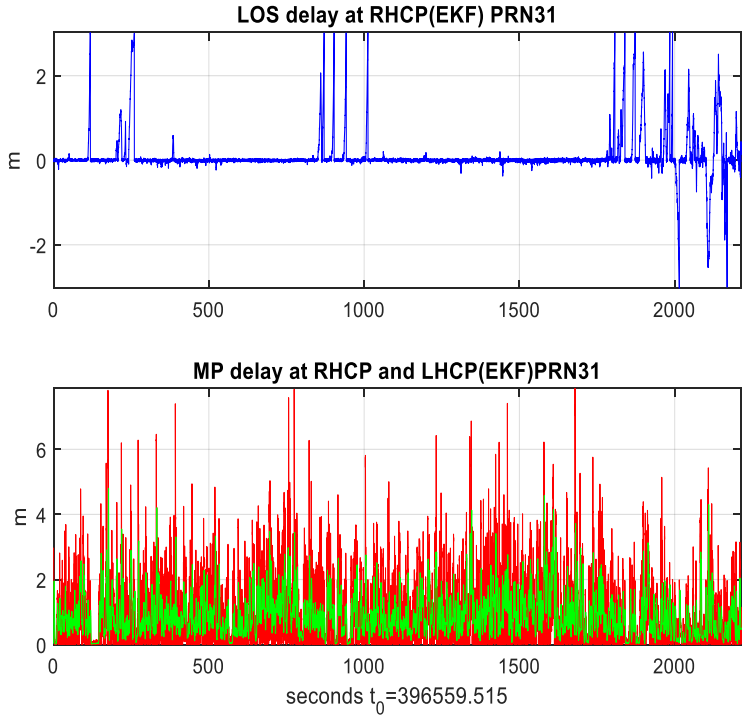

Figure 7-13 : LoS and multipath delay estimation

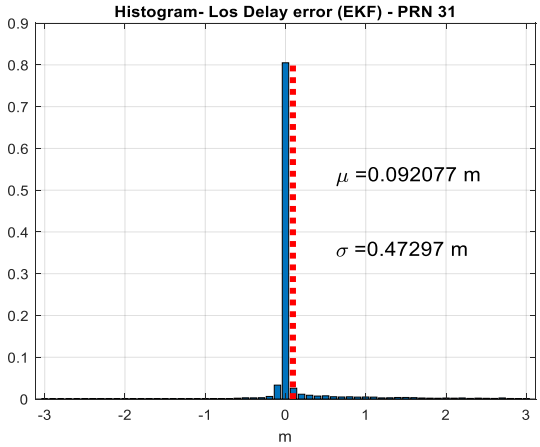

Figure 7-14 : Histogram LoS Delay

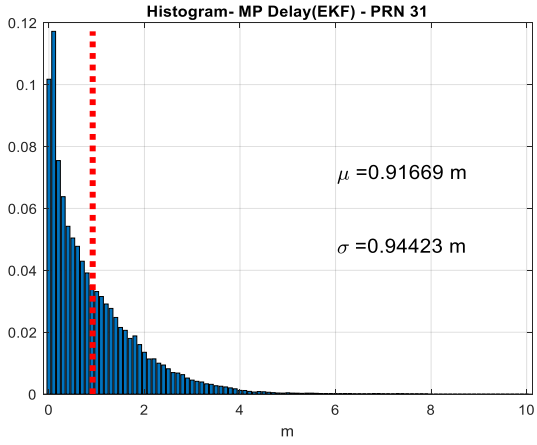

Figure 7-15 : Histogram multipath delay

In the histogram shown by figure 7.14 we can see that the estimated LoS delay is mostly around zero. This implies that the estimated error between the tracked LoS delay and the actual LoS delay is always around zero. Instead the histogram in figure 7.15 shows that the Multipath delay is always positive as expected and the distribution seems to fit a negative exponential one with a mean value equal to 0.92 m.

Apart from the above estimates, the ratio between the desired (LoS) and undesired (MP)signal is estimated for both the RHCP and LHCP.

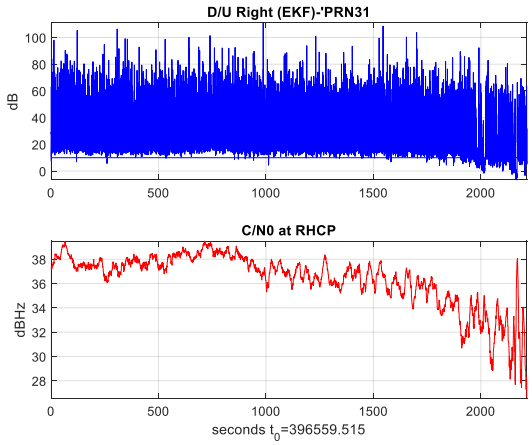

Figure 7-16 : D/U RHCP

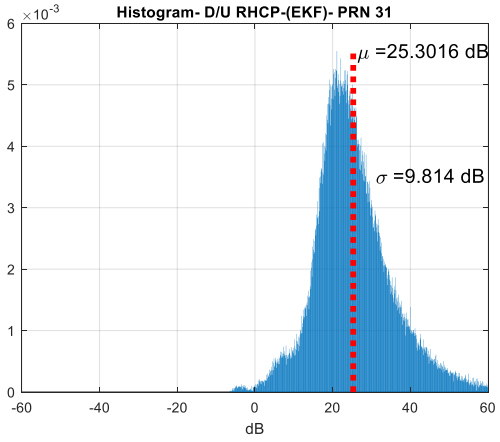

Figure 7-17 : Histogram D/U RHCP

The D/U at the RHCP is defined as the ratio of the LoS signal amplitude and multipath signal amplitude referred to as desired and undesired signal respectively. Mathematically,

$$(D\ /\ U)_R = 20\log_{10}\left(\frac{\alpha_{LOS}^{RR}}{\alpha_{MP}^{R}}\right)$$

where,

$$\alpha_{LOS}^{RR} = LOS\ amplitude\ in\ RHCP\ chain$$

$$\alpha_{MP}^{R} = Multipath\ amplitude\ in\ RHCP\ chain$$

It can be seen in the histogram of the D/U at RHCP that the desired signal (LoS) is almost always high compared to the undesired signal (multipath) which means the RHCP is always tracking high LoS power. The negative D/U in the histogram at some instants show the presence of higher undesired signal (multipath) than the desired signal (LoS signal). This can also be seen in the figure of D/U estimation where towards the end the D/U is negative and that is the region where we discussed the possible presence of multipath in previous analysis. This is a very interesting observation because we speculated from the analysis of the code errors and pseudorange biases the possible presence of multipath after the 2000th second.

Similarly, for the LHCP chain we can observe the D/U in the following figures

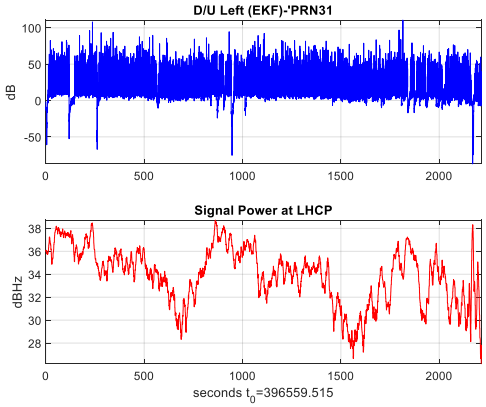

Figure 7-18 : D/U LHCP

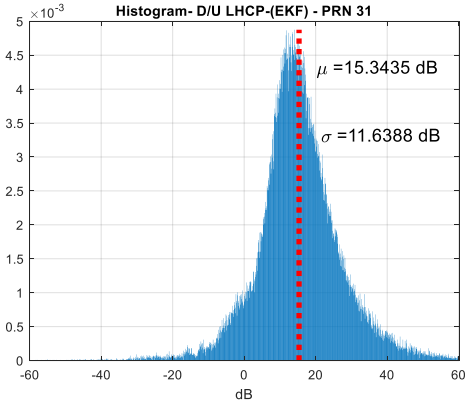

Figure 7-19 : Histogram D/U LHCP

The D/U at the LHCP is defined as the ratio of the LoS signal and the Multipath signal tracked by the LHCP antenna. Mathematically,

$$(D\ /\ U)_L = 20\log_{10}\left(\frac{\alpha_{LOS}^{LR}}{\alpha_{MP}^{L}}\right)$$

where,

$$\alpha_{LOS}^{LR} = LOS\ amplitude\ in\ LHCP\ chain$$

$$\alpha_{MP}^{L} = Multipath\ amplitude\ in\ LHCP\ chain$$

In the above figures we can see that the D/U at the LHCP is mostly positive but there are more instances than in the RHCP chain where the D/U is negative which could mean the presence of multipath component that is being tracked by the LHCP chain.

The statistical characterisation of the ratios between the multipath signal amplitude on the RHCP and LHCP chain with respect to the LoS on the RHCP chain are reported in figure 7-24 and figure 7-25 respectively with the normalised histograms(i.e. probability density functions)

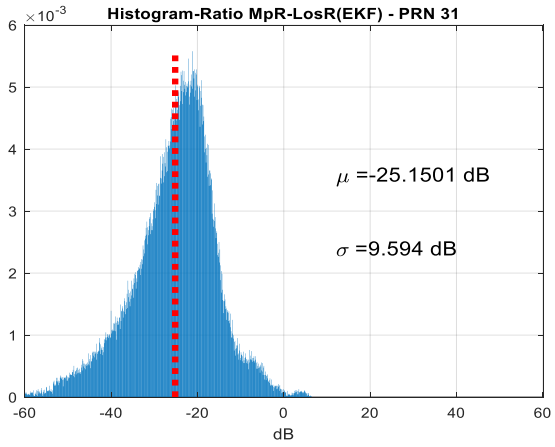

Figure 7-20 : Histogram ratio(A_{MP}^{R}/A_{LoS}^{RR})

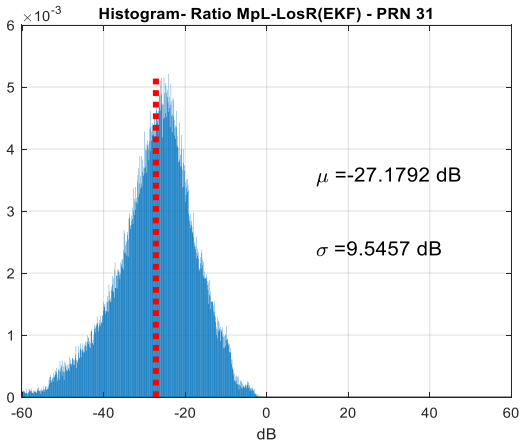

Figure 7-21 : Histogram ratio(A_{MP}^{L}/A_{LoS}^{RR})

From the histogram in figure 7-20 we can say that the LoS amplitude estimated in the RHCP chain is always higher than the multipath signal estimated of the same chain. There are some

intervals where the multipath amplitude is higher than the LoS signal amplitude (i.e. ratio higher than 0 with low probability).

From the histogram in figure 7.21 it can be noted that the LoS signal is always higher than the multipath estimated at the LHCP chain.

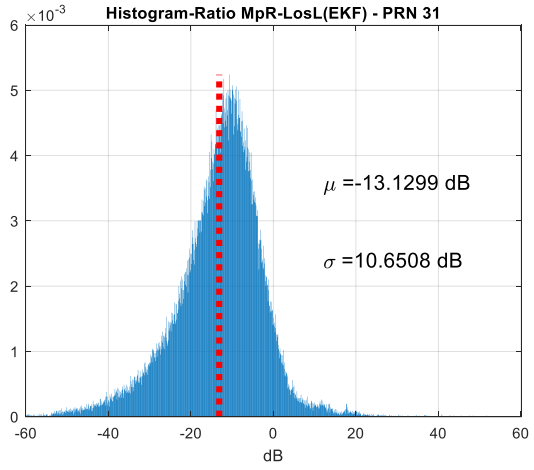

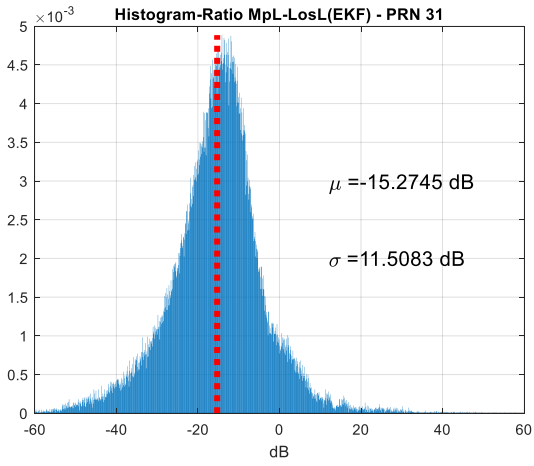

Figure 7-22 : Histogram ratio (A_{MP}^{R}/A_{LoS}^{LR})

Figure 7-23 : Histogram ratio(A_{MP}^{L}/A_{LoS}^{LR})

In the above two histograms , the ratios with respect to the LoS amplitude at the LHCP chain to compare the multipath powers with respect to the cross-polar LoS contribution at LHCP chain. In these cases, even the LoS signal is received in cross-polar mode, its estimated power at correlators is higher than the multipath ones. This can be justified by the fact that the multipath is received after reflection and from negative angles, whereas the LoS is received on the positive angle and so amplified more than the multipath replica.

7.1.2 Constrained EKF Estimations

In this section the results obtained by constraining the EKF processing the same PRN-31 is reported. The evolution of innovation using the constrained EKF can be seen as below

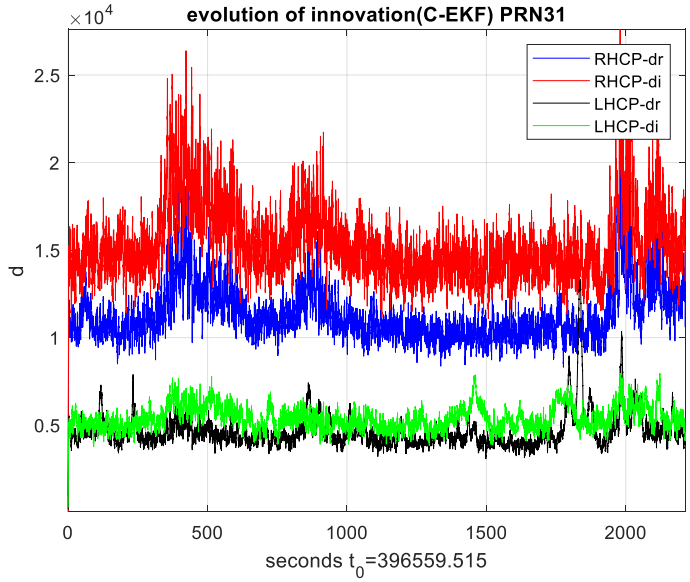

Figure 7-24 : Evolution of innovation

The evolution of innovation is almost the same as the previous case, but we can see that the innovation for the LHCP side is very low compared to the innovation of the RHCP side. This is because of the difference in magnitudes of the observables.

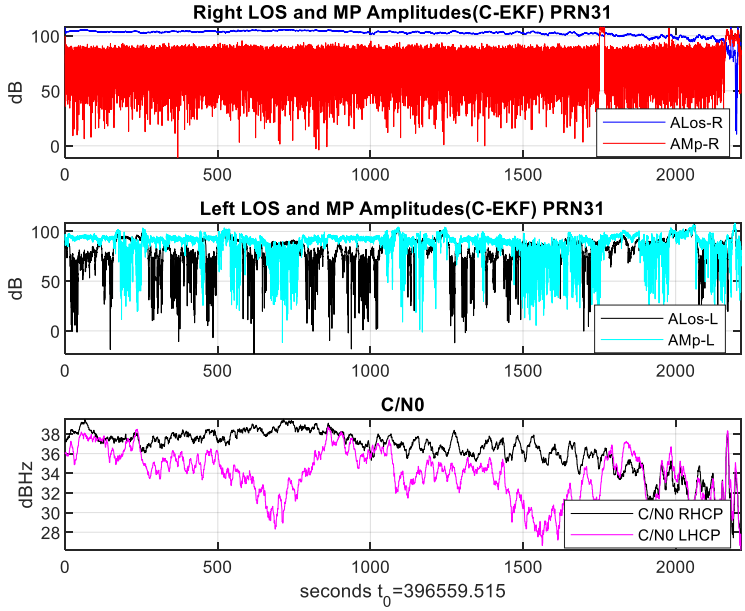

Figure 7-25 : LOS and multipath amplitudes in dB

From the figure 7-25 which presents the estimated LoS and multipath amplitudes, we can see the presence of multipath towards the end of the database.

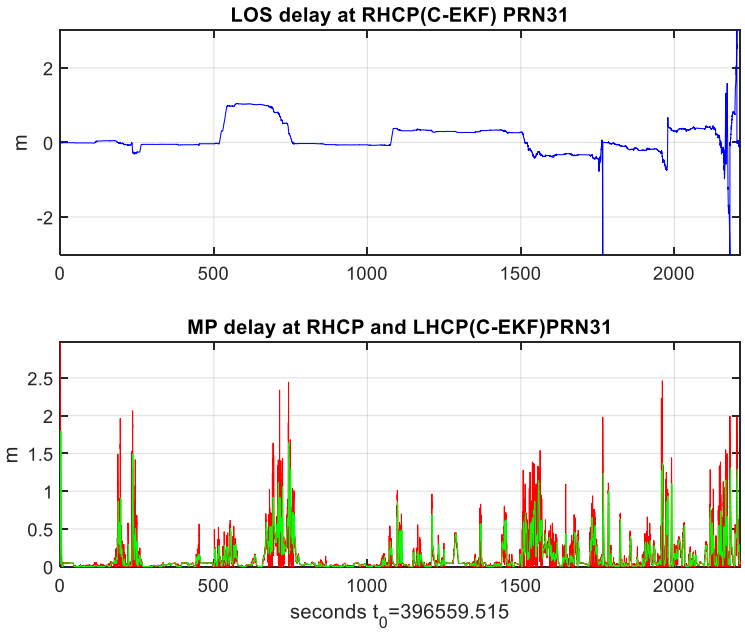

Figure 7-26 : Estimated LOS and MP delay

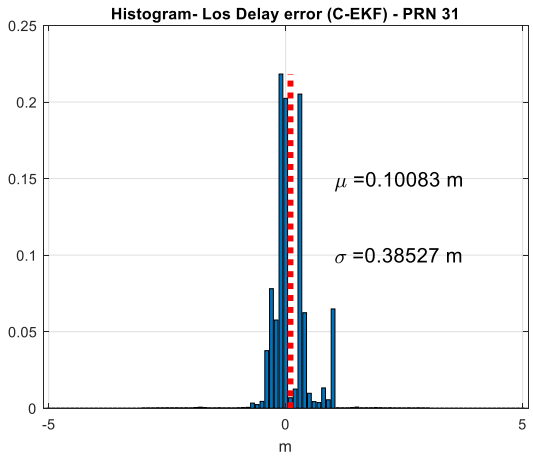

Figure 7-27 : Histogram for LOS delay error

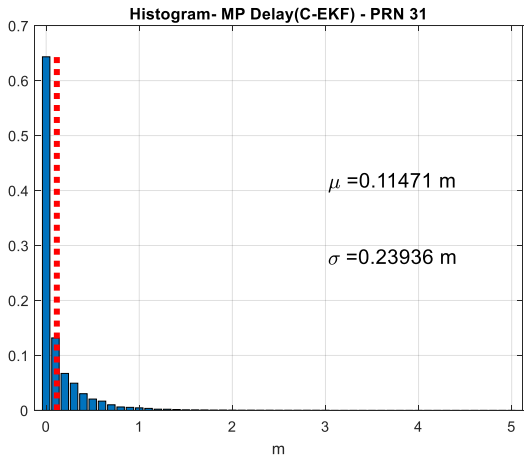

Figure 7-28 : Histogram for Multipath Delay

The histogram in figure 7-27 illustrates that the LoS delay is almost always around zero which means the estimated error between the tracked LoS delay and actual LoS delay are almost always perfectly aligned. Figure 7-28 shows that the multipath delay is always positive by

definition and the distribution seems to fit a negative exponential one, with a mean value equal to 0.11 m.

We can observe the ratios between desired and undesired signals for the case of Constrained EKF for both the RHCP and LHCP chain in the following figures

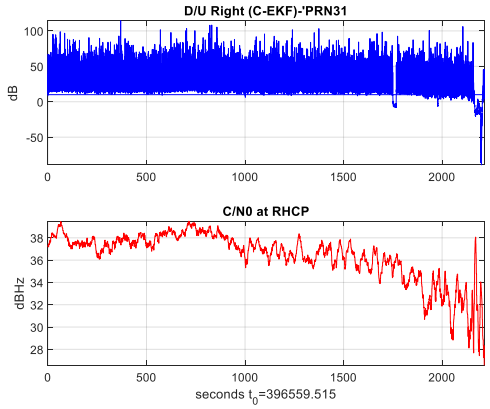

Figure 7-29 : D/U estimation at RHCP

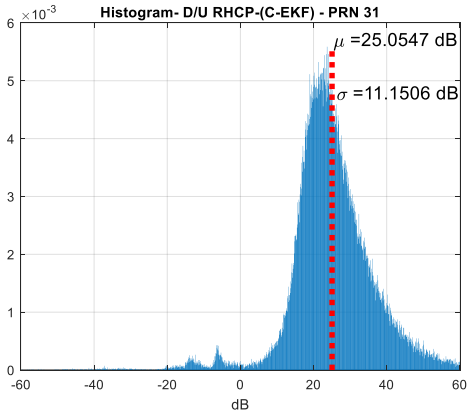

Figure 7-30 : Histogram for D/U at RHCP

For the Constrained EKF, the D/U RHCP histogram suggests that the RHCP chain is tracking the LoS (desired signal) and there are only few instances where the multipath signal (undesired signal) is higher than the LoS. This is also evident in the D/U plot vs time.

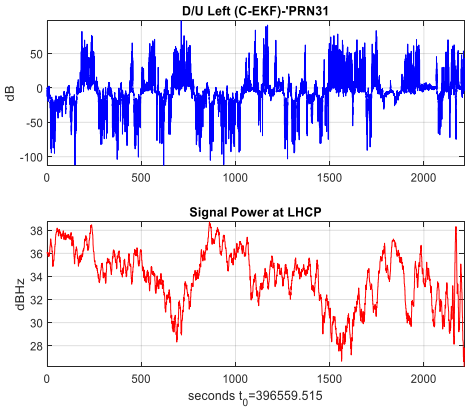

Figure 7-31 : D/U estimation at LHCP

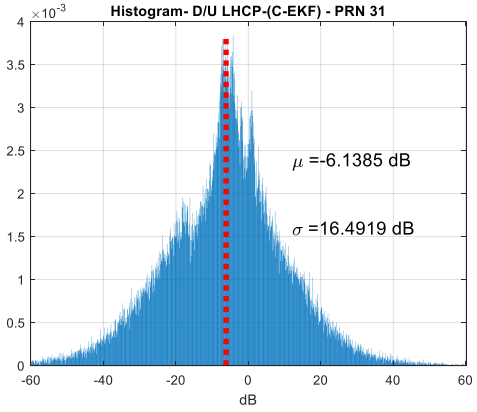

Figure 7-32 : Histogram for D/U at LHCP

From the histogram for LHCP chain, we can see that the tracked undesired signal is higher than the LoS signal in 50% of the time, suggesting the multipath signal being tracked by the LHCP chain with high probability.

The statistical characterisation of the ratios between the multipath amplitude on the RHCP and LHCP chain with respect to the LoS on the RHCP chain in case of Constrained EKF are reported in figures 7-33 and figures 7-34 respectively with the normalised histograms (i.e. probability density functions). Similarly, the histograms for the ratios between the multipath amplitude at the RHCP and LHCP chains with respect to the LoS in RHCP chain is presented in figures 7-35 and 7-36 respectively.

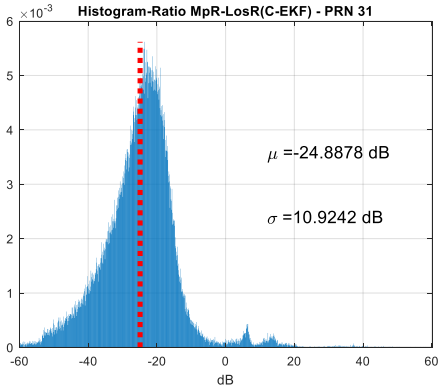

Figure 7-33 : Histogram ratio(A_{MP}^{R}/A_{LoS}^{RR})

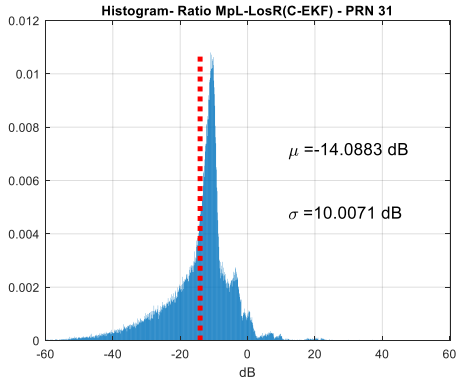

Figure 7-34 : Histogram ratio(A_{MP}^{L}/A_{LoS}^{RR})

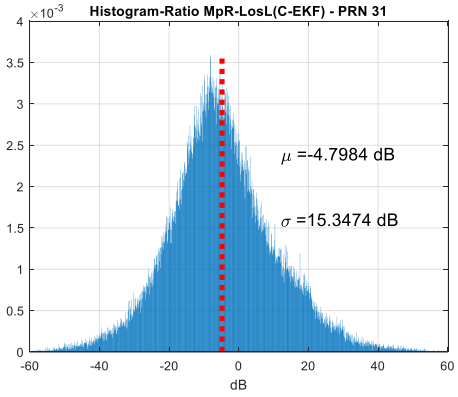

Figure 7-35 : Histogram ratio (A_{MP}^{R}/A_{LoS}^{LR})

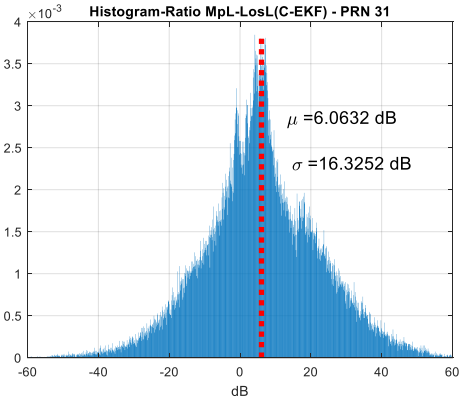

Figure 7-36 : Histogram ratio(A_{MP}^{L}/A_{LoS}^{LR})

If compared to EKF, the Constrained EKF results show similar results for the RHCP chain, whereas for the LHCP D/U large differences are shown for the LHCP components.

The use of constrained EKF can be much more efficient than the legacy EKF when applying an averaging process on the observables, considering that the two applied constrains are much valid as long is the integration/average time considered (i.e. DLL output is on average zero).

We chose to plot the ratios shown in figures 7.32 to 7.35 to see if there is the presence of multipath on a site and if yes at what level. It also helps to understand which amplitude component is higher among the 4 i.e. the Right Multipath, Right LoS, Left Multipath and left LoS that helps in understanding the severity of the multipath contamination.

We can also select a set of thresholds to characterize different levels of multipath conditions on a site: low, medium, high in order to select the site for certain applications.

8 CONCLUSION AND FUTURE WORK

In this work after a brief review of the state-of the art techniques for multipath mitigation and estimation, the EKF scheme was chosen for the multipath parameter's estimation. The method adopted works in an open loop mode without providing any feedback to the High Sensitive Receiver. The overall setup consists of a Dual Polarised Antenna , a High Sensitive navigation multicorrelators receiver and the toolbox itself. With this scheme working at the post-correlation level the multicorrelators observables coming from both RHCP and LHCP chains were used. This facilitated a diversity gain due to the use of Dual Polarised antenna. The RHCP and LHCP observables along with the multipath parameters were modelled in order to fit in the working principle of EKF that includes the stages of prediction and correction. The RHCP and LHCP signal model has common parameters which makes number of parameters to be estimated not increasing so much w.r.t. the number of additional available observables. However, the number of parameters comes out from a trade-off between model accuracy and complexity. Anyway, it is worth to be noted that, to have both RHCP and LHCP an increased hardware and processing complexity is intrinsically required.

After the data is passed through the EKF for estimation, a series of charts depicting the evolution of estimated states along time and the histograms for statistical analysis are generated and reported in the thesis. The charts include the representation of the estimated LoS and multipath signal amplitudes, LoS and multipath delay for both the RHCP and LHCP chains. In addition to this, other figures of merit like the D/U ratios (the ratio between the desired and undesired signals) along with the histogram are reported and discussed. A statistical characterisation of the ratios between the multipath amplitudes on RHCP and LHCP chains with respect to the LoS amplitudes

on the RHCP and LHCP chains are presented and discussed. After the analysis it was concluded that there are some instants where there is the presence of multipath especially at low elevation angles. For the verification the code errors of the same PRN for both the RHCP and LHCP chains generated using the multipath survey feature of the toolbox was analysed that also indicated the presence of multipath in the same region as indicated by the EKF estimation. Additionally, the analysis of measured C/No's and the analysis of whole set of multicorrelator values (i.e. 11) focusing on specific observation times showed the presence of multipath.

Furthermore, along with the conventional EKF a constrained version of the EKF is also implemented and analysed in the thesis work. The same sets of charts and histograms are generated and explained in this case as well producing similar results.

The limitation of the work performed in this thesis is that the algorithm implementation and estimation is done only in the real data due to the unavailability of the data generated in a simulated environment. A possible future work would be to verify the algorithm performance also in a more controlled environment, considering different types of multipath in terms of D/U, delay and period.

9 BIBLIOGRAPHY

[1] A. Emmanuele, M. Puccitelli, N. Pastori, A. Ferrario, L. Marradi, A. Khanal, P. Crosta, R. Sarnadas, T. Thúróczy, R. Guidi, "*Innovative Toolbox for Reference Station Multipath and Interference Site Surveying,*" *Proceedings of 32nd International Technical Meeting of the Satellite Division of the Institute of Navigation*, Sept. 16-20, 2019, Miami, Florida, USA.

[2] "Galileo", European GNSS, European GNSS Agency (GSA), 21 May 2019, https://www.gsa.europa.eu/european-gnss/galileo/galileo-european-global-satellite-based-navigation-system

[3] "GNSS Error Sources", An Introduction to GNSS, NovAtel Inc., Hexagon Positioning Intelligence, https://www.novatel.com/an-introduction-to-gnss/chapter-4-gnss-error-sources

[4] Michael S. Braasch, "Multipath" *Springer Handbook of Global Navigation Satellite Systems*, Peter J.G. Teunissen, Oliver Motenbruck. Cham: *Springer International Publishing* AG, 2017

[5] F. Dovis, "GPS SIS SatNavSys_updated," Satellite Navigation Systems, 2017, Politecnico di Torino. Microsoft PowerPoint presentation.

[6] Navipedia GPS signal plan, *[https://gssc.esa.int/navipedia/index.php/GPS_Signal_Plan]*

[7] Yang, Chun, Porter, Alec, "GPS Multipath Estimation and Mitigation Via Polarization Sensing Diversity: Parallel Iterative Cross Cancellation," *Proceedings of the 18th International Technical Meeting of the Satellite Division of The Institute of Navigation (ION GNSS 2005*), pp. 2707-2719 Sept 2005*,* Long Beach, CA, USA

[8]. F. Dovis, "Galileo and BOC signals," Satellite Navigation Systems, 2017, Politecnico di Torino. Microsoft PowerPoint presentation.

[9]. "GNSS Solutions: Atomic clocks on satellites and mitigating multipath", *InsideGNSS*, Sept. 2006

[10]. R. Chaggara, C. Macabiau, E. Chatre, "Using GPS Multicorrelator Receivers for Multipath Parameters Estimation" *Proceedings of the 15th International Technical Meeting of the Satellite Division of The Institute of Navigation (ION GPS 2002),* pp. 477-492*,* Sept. 2002*,* Portland, OR, USA

[11]. A. Izadpanah, "Parameterization of GPS L1 Multipath Using a Dual Polarized RHCP/LHCP Antenna," Ph.D. Thesis, University of Calgary, Calgary, AB, Canada, 2009.

[12] Groves, P.D.; Jiang, Z.; et al., "Novel Multipath Mitigation Methods using a Dual-Polarization Antenna," *Proceedings of the 23rd International Technical Meeting of the Satellite Division of the Institute of Navigation*, pp. 140–151, 21–24 Sept. 2010, Portland, OR, USA.

[13] A.H. Mohamed, K. P. Schwarz, “Adaptive Kalman Filtering for INS/GPS,” Journal of Geodesy, May 1999, vol. 73, Issue 8Issue 4, pp. 193-203

[14] M. R. Ananthasayanam, Shyam Mohan M, Naren Naik, R. M. O. Gemson, “A Heuristic Reference Recursive Recipe for the Menacing Problem of Adaptively Tuning the Kalman Filter Statistics,” 27 May 2015

[15] M. Tsagris, C. Beneki, H. Hassani, “On the folded normal distribution,” *Mathematics 2014, 2(1), 12-28*; *[https://doi.org/10.3390/math2010012]*

[16] D. Simon, “Kalman filtering with state constraints: a survey of linear and nonlinear algorithms,” *IET Control Theory and Applications,* 2009, vol. 4, Issue 8, pp. 1-16, *[https://academic.csuohio.edu/simond/pubs/IETKalman.pdf]*